Uncertain spatial pattern of future land use and land cover change and its impacts on terrestrial carbon cycle over the Arctic-Boreal region of North America

Meng Luo[1], Fa Li[2], Dalei Hao[3], Qing Zhu[4], Hamid Dashti[2], and Min Chen[2]

[1]University of Wisconsin-Madison
[2]University of Wisconsin, Madison
[3]Pacific Northwest National Laboratory
[4]Lawrence Berkeley National Laboratory (DOE)

March 16, 2023

Abstract

Land use and land cover change (LULCC) represents a key process of human-Earth system interaction and has profound impacts on ecosystem carbon cycling. As a key input for ecosystem models, future gridded LULCC data is typically spatially downscaled from regionally LULCC projections by integrated assessment models. The uncertainty associated with different spatial downscaling methods and its impacts on subsequent model projections have been historically ignored and rarely examined. This study investigated this problem using two representative spatial downscaling methods and focused on the impacts on the carbon cycle over ABoVE domain. Specifically, we used the Future Land Use Simulation model (FLUS) and Demeter model to generate 0.25-degree gridded LULCC data with the same input of regional LULCC projections from Global Change Analysis Model, under SSP126 and SSP585. The two sets of downscaled LULCC were used to drive CLM5 to prognostically simulate terrestrial carbon cycle dynamics over the 21st century. The results suggest large spatial-temporal differences between two LULCC datasets under both SSP126 and SSP585. The LULCC differences further lead to large discrepancies in the spatial patterns of projected carbon cycle variables, which are more than 79% of the contributions of LULCC in 2100. Besides, the difference for LULCC and carbon flux under SSP126 is generally larger than those under SSP585. This study highlights the importance of considering the uncertainties induced by spatial downscaling process in future LULCC projections and carbon cycle simulations.

Uncertain spatial pattern of future land use and land cover change and its impacts on terrestrial carbon cycle over the Arctic–Boreal region of North America

Meng Luo[1], Fa Li[1], Dalei Hao[2], Qing Zhu[3], Hamid Dashti[1], Min Chen[1]

[1]Department of Forest and Wildlife Ecology, University of Wisconsin-Madison, Madison, WI, USA.

[2]Atmospheric Sciences and Global Change Division, Pacific Northwest National Laboratory, Richland, WA, USA

[3]Climate and Ecosystem Sciences Division, Lawrence Berkeley National Laboratory, Berkeley, CA, USA.

Corresponding author: Min Chen (mchen392@wisc.edu)

Key Points:

- We identified a traditionally ignored source of uncertainty in model projected carbon cycle from the future land use and land cover change (LULCC) data.
- Spatial downscaling is a necessary step for generating gridded LULCC data, but different downscaling methods may lead to results with large spatial differences.
- The impacts of using different spatial downscaling methods are more than 79% of the contributions of future LULCC to carbon cycle projections in 2100.

Abstract

Land use and land cover change (LULCC) represents a key process of human-Earth system interaction and has profound impacts on terrestrial ecosystem carbon cycling. As a key input for ecosystem models, future gridded LULCC data is typically spatially downscaled from regional LULCC projections by integrated assessment models, such as the Global Change Analysis Model (GCAM). The uncertainty associated with the different spatial downscaling methods and its impacts on the subsequent model projections have been historically ignored and rarely examined. This study investigated this problem using two representative spatial downscaling methods and focused on their impacts on the carbon cycle over the Arctic-Boreal Vulnerability Experiment (ABoVE) domain where extensive LULCC is expected. Specifically, we used the Future Land Use Simulation model (FLUS) and the Demeter model to generate 0.25-degree gridded LULCC data (i.e., $LULCC_{FLUS}$ and $LULCC_{Demeter}$, respectively) with the same input of regional LULCC projections from GCAM, under both the low (i.e., SSP126) and high (i.e., SSP585) greenhouse gas emission scenarios. The two sets of downscaled LULCC were used to drive the Community Land Model version 5 (CLM5) to prognostically simulate the terrestrial carbon cycle dynamics over the 21st century. The results suggest large spatial-temporal differences between $LULCC_{FLUS}$ and $LULCC_{Demeter}$, and the spatial distributions of the needleleaf evergreen boreal tree, broadleaf deciduous boreal tree, broadleaf deciduous boreal shrub, and C3 arctic grass are particularly different under both SSP126 and SSP585. The LULCC differences further lead to large discrepancies in the spatial patterns of projected gross primary productivity, ecosystem respiration, and net ecosystem exchange, which are more than 79% of the contributions of future LULCC in 2100. Besides, the difference for LULCC and carbon flux under SSP126 is generally larger than those under SSP585. This study highlights the importance of considering the uncertainties induced by the spatial downscaling process in future LULCC projections and carbon cycle simulations.

Plain Language Summary

Land use and land cover change (LULCC) affects the carbon cycle in ecosystems. To predict future LULCC and carbon cycle changes, scientists use spatial downscaling methods to create detailed LULCC maps. However, different methods can lead to different results and can impact carbon cycle projections. Our study found that using different spatial downscaling methods can lead to a large portion of the uncertainty in future LULCC and carbon cycle projections over the Arctic-Boreal region. It is important to consider these uncertainties when studying future changes in land use and carbon cycling.

1 Introduction

Land use and land cover change (LULCC) represents a key human impact on the Earth system (Chen et al., 2019). It has crucial impact on many important ecological, biophysical, biogeochemical and climatic processes such as biodiversity (Semenchuk et al., 2022), energy balance (Duveiller et al., 2018; Dashti et al., 2022), carbon and water cycle (Harris et al., 2021; Friedlingstein et al., 2021; Sterling et al., 2013), and climate extremes (Findell et al., 2017). Substantial LULCC has occurred in the past several decades (Song et al., 2018; J. Liu et al., 2020) and is expected to continue in the future (Doelman et al., 2018; Friedlingstein et al., 2021; Chen et al., 2020b; Bukovsky et al., 2021). Under global climate change, the Arctic-Boreal Vulnerability Experiment (ABoVE) domain is a vulnerable hotspot region, due to the amplified warming (Liu et al., 2020), and has been used as a key representative region to understand the changes in the whole Arctic. Extensive LULCC has been observed by satellites in this region (Alcaraz-Segura et al., 2010), such as the shrub expansion and forest cover change (Alcaraz-Segura et al., 2010; Pastick et al., 2019). Previous study found the historical LULCC over this region has large impacts on carbon cycle (Mekonnen et al., 2021). Projecting and understanding how future LULCC will evolve and its ecological impacts over the ABoVE domain are of vital importance for making mitigation and adaptation strategies and sustainable management of ecosystems in this region and the whole high-latitude area.

Gridded LULCC projection is essential to analyze the spatial patterns of LULCC and to understand the impact of LULCC on important ecosystem services, e.g., carbon sequestration, in the future. Integrated Assessment Models (IAMs) are commonly used to project future LULCC under diverse global change scenarios. However, these IAM projections are usually under large political, economic, or geographical region level, and spatial downscaling is a necessary step to obtain a spatially explicit LULCC data (i.e. gridded LULCC) from the IAM projections. Recent studies have investigated the large uncertainties in the future gridded LULCC due to the difference in interpretations of narratives, model assumptions, and structure of IAMs (Riahi et al., 2017; Guivarch et al., 2022) as well as the difference in spatial resolution (Alexander et al., 2017) and LULCC definitions (Chen et al., 2020b). For instance, the computable-general equilibrium models such as the Global Change Analysis Model (GCAM) (Calvin et al., 2017, 2019), have a smaller area of projected cropland in the last half of the 21st century than the partial equilibrium models (Alexander et al., 2017) like the Model of Agricultural Production and its Impact on the Environment (MAgPIE; Popp et al., 2014), despite both models are among the major IAMs in the world. These uncertainties could propagate and result in large uncertainties in the following analyses of LULCC impacts, such as the quantification of critically important terrestrial ecosystem carbon cycle (Di Vittorio et al., 2018) in Earth System Models.

However, as a key step of generating gridded LULCC data, spatial downscaling also has large uncertainties that, to the best of our knowledge, have received limited attention. The difference in the downscaled LULCC due to different spatial downscaling methods remains underexplored and it is unclear how big the difference could be. Several spatial downscaling methods, e.g., Demeter (Chen et al., 2019; Chen et al., 2020b; Vernon et al., 2018), FLUS (Dong et al., 2018; Cao et al., 2010; Luo et al., 2022), Global Land-use Model 2 (Ma et al., 2019; Hurtt et al., 2020), and Platform for Land-Use and Environmental Model (Wu et al., 2019; Fujimori et al., 2018), have been widely used to disaggregate regional LULCC projections from IAMs. Although these models/methods can take in the same regional LULCC projections from the same IAM, their mechanisms of disaggregating the areal projection into grid levels are different. For instance, Demeter uses the proximal relationships defined by kernel density probabilities to process the intensification and expansion of LULCC (Vernon et al., 2018), while FLUS combines the artificial neural networks (ANN) and the mechanisms of cellular automata (CA) (Liu et al., 2017) to couple both human-related and natural environmental effects and consider the interactions and competition among different land types. These differences are expected to cause diverse spatial patterns of future LULCC projections, which could further influence the subsequent projections of terrestrial ecosystem carbon fluxes, such as the gross primary productivity (GPP), ecosystem respiration (ER), and their difference net ecosystem exchange (NEE; NEE=ER-GPP).

This study focuses on the future LULCC and carbon fluxes in the ABoVE domain under two Shared Socioeconomic Pathways (SSPs), i.e., SSP126 and SSP585). We aim to answer two questions: 1) how much uncertainty of the spatial pattern of LULCC could be caused by different spatial downscaling methods and 2) what are the impacts on the subsequent projections of ecosystem carbon fluxes with the uncertain downscaled LULCC? For this purpose, we used two different spatial downscaling methods (i.e., Demeter and FLUS) to generate 0.25-degree gridded LULCC data with the same LULCC classification and definitions based on the same regional projections from GCAM from 2015 to 2100. We then used the Community Land Model version 5 (CLM5) to simulate the carbon fluxes driven by the gridded LULCC data produced by Demeter and FLUS, respectively. Thereby, we quantified the differences of gridded LULCC generated by Demeter and FLUS and their impacts on future GPP, ER, and NEE projections.

2 Materials and Methods

2.1 Demeter and FLUS

Demeter is a LULCC spatial disaggregation model developed as part of the GCAM software ecosystem and could be extended to other IAMs (Vernon et al., 2018). It uses an intensification and expansion strategy (Page et al., 2016; West et al., 2010) to perform the spatial downscaling, following a series of user-defined rules. Specifically, the treatment order defines final land type is downscaled first. Transition priorities define what type of land swaps are favored. Spatial constraints, e.g., kernel density, measure the probability density of a land type around a given grid cell. The soil workability and nutrient availability help to indicate suitability for agriculture. Detailed algorithms and optimization procedures can refer to the previous studies (Chen et al., 2019; Vernon et al., 2018).

FLUS is a CA-based model which can be used to explore nonlinear relationships between the complex spatial factors and multiple land types (Liu et al., 2017; Liao et al., 2020). FLUS first estimates the probability of occurrence for each LULCC on each grid cell based on ANN. Then FLUS accounts for the competition and interactions among different land types and carries out the land allocation by combining the probability-of-occurrence, user-defined conversion cost, neighborhood condition, and competition among different land types and the mechanisms of CA, self-adaptive inertia, and competition mechanism. During this stage, the land type with a higher probability-of-occurrence is more likely to be predicted as the target land type, while those with a relatively lower probability-of-occurrence can still be possibly converted based on the roulette selection mechanism.

2.2 Data preparation for LULCC spatial downscaling

We used the regional LULCC projections under both the low (i.e., SSP126) and high (i.e., SSP585) emission scenarios derived from GCAM (Chen et al., 2020b) as the input for the spatial downscaling (Figure S1). SSP126 describes a sustainability scenario pathway with an increase of global mean temperature by 1.5°C to 2 °C compared to the pre-industrial level by the end of the 21st century. SSP585 describes a world that widely uses fossil-fuels and the global mean temperature increase by about 4.4 °C by the end of the 21st century. Under both scenarios, GCAM projects LULCC at 5-year time step over 2015-2100 in 384 regions globally, ten of which locate in the ABoVE domain (Figure 1).

Both Demeter and FLUS require a gridded land cover map at the target spatial resolution as the reference for their spatial disaggregation, and here we used the year 2015 land cover map at a spatial resolution of 500m provided by the MODerate resolution Imaging Spectroradiometer (MODIS) land cover product (MCD12Q1 C6). Specifically, we used the Plant Functional Types

(PFT) classification in MCD12Q1 (hereafter referred to MODIS_PFT) (Friedl et al., 2010), which classifies the global land surface into 11 types. However, MODIS_PFT is different from the land classification system of GCAM and that of the downstream land surface model CLM5 (CLM5_PFT) (Lawrence et al., 2019). Therefore, a few reclassification steps (Figure S2) were applied to harmonize the differences, following a similar strategy used in the previous studies (Chen et al., 2020b; Luo et al., 2022).

Specifically, Demeter allows inconsistent classification systems among the input (GCAM), reference map (MODIS_PFT) and the target (CLM_PFT). The spatial downscaling can be performed with Demeter once the links among the three classification systems are defined. In contrast, the design of FLUS requires an identical land cover type classification system across input, reference and target. Therefore, we first consolidated both GCAM and MODIS_PFT type into 7 broad types and built a reclassification scheme (Table 1) for the harmonization. For Demeter, we reclassified the 11-type 500m MODIS land cover map into 18 CLM5_PFT types (Figure 1) based on the climate-based rules as described in Bonan et al. (2002), using the WorldClim V2 monthly climatological temperature and precipitation data (Fick & Hijmans, 2017). The reclassified 500 m MODIS data was then aggregated to 0.25 degree to be used as the reference map for Demeter downscaling in this study. For FLUS, we reclassified the MODIS reference land cover map to a new reference map with the 7 broad types. Spatial downscaling with FLUS thus generated LULCC data in the same 7 broad types, and we finally mapped the 7 broad types into the 18 CLM5_PFT types by using a similar strategy in a previous study (Chen et al., 2020a) that iteratively assign the new label of the nearest neighbor for each map grid in each year. It must be noted that the differences in these preprocessing steps are also an inherent uncertainty source of the gridded LULCC products while using different spatial downscaling models.

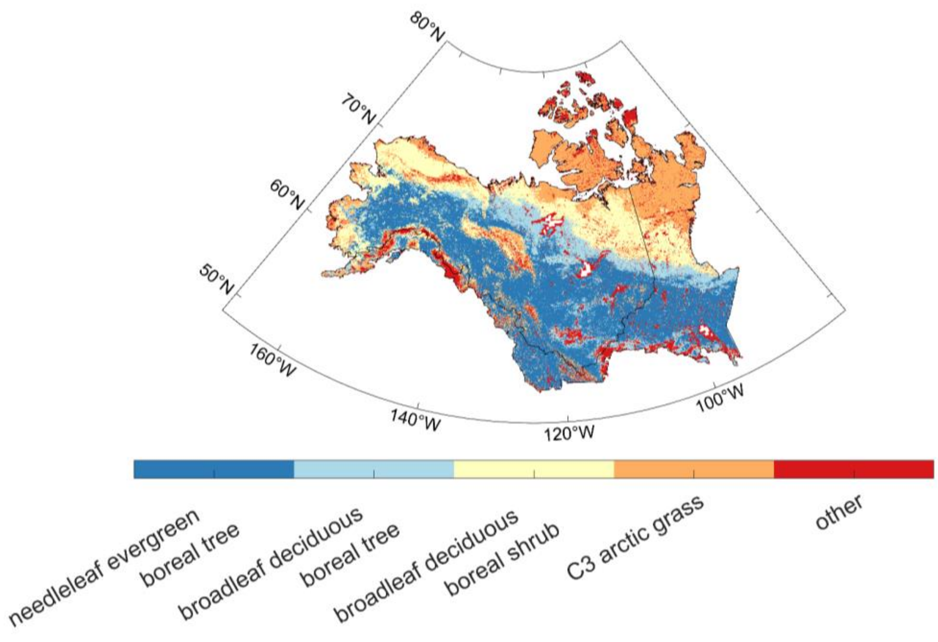

Figure 1. The spatial distribution of LULCC over the ABoVE domain in 2015. Different colors represent different CLM5_PFT types**.**

In addition, due to the errors in the geographical data (Chen et al., 2020b; Luo et al., 2022) used in GCAM, the geographical areas between GCAM regional projections and MODIS reference map are not consistent and also need to be harmonized. Specifically, for Demeter, we used the Eq. (1) to harmonize the LULCC projections (Chen et al., 2020b):

$$A_{GLT,u,H}(t) = \begin{cases} A_{BLT,u,B}(t) \times \frac{A_{GLT,u,G}(t)}{A_{BLT,u,G}(t)} & t = 2015 \\ A_{GLT,u,H}(t-1) \times \frac{A_{GLT,u,G}(t)}{A_{GLT,u,G}(t-1)} & 2020 \leq t \leq 2100 \end{cases} \tag{1}$$

where $A_{GLT,u,H}(t)$ is the harmonized area in region *u* in year t for each GCAM type (GLT). $A_{BLT,u,B}(t)$ is the area in region *u* in the reference map in year *t* for each broad type (BLT). $A_{GLT,u,G}(t)$ is the area in region *u* from GCAM projections in year *t* for each GLT. $A_{BLT,u,G}(t)$ is the area in region *u* from GCAM projection for each BLT in year *t*.

Considering that FLUS uses the broad land types during the spatial downscaling process, we used Eq. (2) to harmonize the regional area between GCAM and the reference map (Luo et al., 2022):

$$A_{BLT,u,H}(t) = \begin{cases} A_{BLT,u,B}(t) & t = 2015 \\ A_{BLT,u,H}(t-1) \times \frac{A_{BLT,u,G}(t)}{A_{BLT,u,G}(t-1)} & 2020 \leq t \leq 2100 \end{cases} \tag{2}$$

where $A_{BLT,u,H}$ is the harmonized area in region *u* for each BLT. Such area harmonization for Demeter and FLUS makes sure that the input LULCC projections are adjusted to match the reference map and be consistent in our Demeter and FLUS experiments.

Table 1. *LULCC reclassification scheme for GCAM type, Broad type, MODIS_PFT, and CLM5_PFT.*

GCAM type	Broad type	MODIS_PFT	CLM5_PFT
RockIceDesert	Barren	Barren	Barren
biomass-grass_IRR, biomass-grass_RFD, biomass-tree_IRR, biomass-tree_RFD, Corn_IRR, Corn_RFD, FiberCrop_IRR, FiberCrop_RFD, FodderGrass_IRR, FodderGrass_RFD, FodderHerb_IRR, FodderHerb_RFD, MiscCrop_IRR, MiscCrop_RFD, OilCrop_IRR, OilCrop_RFD, OtherArableLand, OtherGrain_IRR, OtherGrain_RFD, Root-Tuber_IRR, Root-Tuber_RFD, SugarCrop_IRR, SugarCrop_RFD, Wheat_IRR, Wheat_RFD,	Cropland	Cereal Croplands, Broadleaf Croplands	Crop
Forest, Unmanaged Forest	Forest	Evergreen Needleleaf Trees	Needleleaf evergreen temperate tree, Needleleaf evergreen boreal tree
		Deciduous Needleleaf Trees	Needleleaf deciduous boreal tree
		Evergreen Broadleaf Trees	Broadleaf evergreen tropical tree, Broadleaf evergreen temperate tree
		Deciduous Broadleaf Trees	Broadleaf deciduous tropical tree, Broadleaf deciduous temperate tree, Broadleaf deciduous boreal tree
Grassland, Tundra, Pasture, Unmanaged Pasture,	Grass	Grass	C3 arctic grass, C3 non-arctic grass, C4 grass,
Shrubland	Shrub	Shrub	Broadleaf evergreen temperate shrub, Broadleaf deciduous temperate shrub, Broadleaf deciduous boreal shrub
UrbanLand	Urban	Urban and Built-up Lands	Urban
None	Water	Water Bodies	Water

2.3 Generating gridded LULCC with Demeter and FLUS

We used two spatial downscaling methods (i.e., Demeter and FLUS) to generate the gridded LULCC data at a 5-year interval from 2015 to 2100, in line with GCAM (Figure S1). For Demeter, key parameters such as the optimal value of the ratio of allocating LULCC as intensification, and threshold percentage of suitable grid cells to accept extensified LULCC allocation used were set as the calibrated values in Chen et al. (2020b). We also used the same treatment order of each land type, and transition priority as that in Chen et al. (2020b). These rules and constraints, together with kernel density probabilities, were used to conduct the intensification and expansion to apply the projected future LULCC allocation. For FLUS, to estimate the probability of occurrence, we first collected the base map in 2015 (see Section 2.2) and 9 spatial factors (shown in Table 2), which reflect different heterogeneous characteristics (i.e., climate, topography, transportation, etc.) related to LULCC (Chen et al., 2020a; Liu et al., 2017; Luo et al., 2022) as the training data for ANN. All these spatial factors were reprojected into 500 m spatial resolution. Other parameters including sampling method, sample rate, and hidden layer were set based on Luo et al. (2022). During the allocation stage, we set the user-defined conversion cost, neighborhood condition, and competition based on the optimal values in Luo et al. (2022). Based on the based map and the abovementioned parameter configuration, we used FLUS to produce 500 m LULCC dataset in the ABoVE domain from 2015 to 2100.

FLUS outputs LULCC at a spatial resolution of 500 m. We aggregated the FLUS outputs into the same resolution as Demeter (i.e., 0.25 degree), and both of them can be used as CLM5. We hereafter refer to two gridded LULCC data produced by Demeter and FLUS as $LULCC_{Demeter}$ and $LULCC_{FLUS}$, respectively. Note that the two datasets are identical in the starting year 2015, since both Demeter and FLUS kept their downscaled maps the same as the reference map in the starting year.

2.4 Projecting future carbon cycle

We used CLM5 to prognostically project the future GPP, ER, and NEE under the two scenarios driven by $LULCC_{Demeter}$ and $LULCC_{FLUS}$, respectively (Figure S1). CLM5 is the land component of the Community Earth System Model version 2.0, which is a state-of-the-art land surface model that mechanistically simulate the biogeophysical, biogeochemical, and ecological processes in the terrestrial environment simultaneously and is an effective tool to quantify impact of LULCC on carbon cycle over a wide range of spatial and temporal scales (Bonan & Doney, 2018; Cheng et al., 2021). Compared to the previous version, CLM5 generally has improved performance in capturing the dynamics of ecosystem carbon cycle (Lawrence et al., 2019).

Specifically, we carried out the CLM5 simulations with biogeochemistry mode for 200 years in an "accelerated decomposition" mode, and subsequently for 400 years in regular spin-up mode by cycling through 2000-2014 to get the steady initial conditions. For the future projections from 2015-2100, we first linearly interpolated the 5-year interval $LULCC_{Demeter}$ and $LULCC_{FLUS}$ into 1-year interval. Then we carried out the future CLM5 simulations using the yearly $LULCC_{Demeter}$, $LULCC_{FLUS}$ from 2015-2100 under both SSP126 and SSP585, respectively. In order to evaluate the impacts of LULCC on future ecosystem carbon cycle, we also carried out another reference 2015-2100 CLM5 simulation with a static land cover in 2015. We hereafter refer to the three sets of GPP, ER, and NEE projections using $LULCC_{Demeter}$, $LULCC_{FLUS}$ and historical LULCC in 2015 as 1) GPP_{FLUS}, ER_{FLUS}, NEE_{FLUS}, 2) $GPP_{Demeter}$, $ER_{Demeter}$, $NEE_{Demeter}$, and 3) $GPP_{Reference}$, $ER_{Reference}$, $NEE_{Reference}$. During the spin-up and future simulations, we used the meteorological forcing data of the Geophysical Fluid Dynamics Laboratory (GFDL) from the standard Inter-Sectoral Impact Model Intercomparison Project phase 3b (ISIMIP3b)(https://www.isimip.org/protocol/3/). The original daily GFDL forcing data was downscaled to 6-hourly based on the diurnal cycle from the Climatic Research Unit - NCEP (CRUNCEP) datasets.

Table 2. *Specifications of the 9 spatial factors used in FLUS during the spatial downscaling process.*

Spatial factor	Period	Spatial resolution	Data source
Annual mean temperature Annual precipitation	Climatological (1970-2000)	0.5'	WorldClim v2.0 (http://www.worldclim.org/)
DEM Slope	1996	1 km	Hengl (2018)
Distance to water	2015	500 m	MODIS PFT (Friedl et al., 2010)
Distance to main roads Distance to highway	1980-2010	500 m	Global Roads Open Access Data Set (gROADS) (https://sedac.ciesin.columbia.edu/data/set/groads-global-roads-open-access-v1/)
Distance to airports	2010	500 m	Huang et al. (2013)Click or tap here to enter text.
Distance to urban centers	2014	500 m	United Nations, Department of Economic Social Affairs, Population Division

2.5 Evaluating the uncertainties of the gridded LULCC dynamics and their impact on future ecosystem carbon cycle

To evaluate the uncertainties induced by two different spatial downscaling methods, we compared the spatial and temporal patterns of $LULCC_{Demeter}$ and $LULCC_{FLUS}$ and the resulted carbon fluxes under SSP126 and SSP585, separately. Here the uncertainties are quantified as the difference in gridded LULCC and carbon fluxes caused by using different LULCC spatial downscaling methods. We calculated the Root Mean Square Deviation (RMSD) and Bias for each CLM5_PFT type between $LULCC_{Demeter}$ and $LULCC_{FLUS}$ to quantify the spatial differences at each year:

$$RMSD_{FLUS,Demeter}^{X} = \sqrt{\frac{\sum_{1}^{N} w_i (X_{FLUS}^{i} - X_{Demeter}^{i})^2}{\sum_{1}^{N} w_i}} \tag{3}$$

$$Bias_{FLUS,Demeter}^{X} = \frac{\sum_{1}^{N} w_i (X_{FLUS}^{i} - X_{Demeter}^{i})}{\sum_{1}^{N} w_i} \tag{4}$$

where N is the number of grid cells, X represents the variables of interest (e.g., fraction of each CLM5_PFT type, GPP, ER, or NEE), the subscript of X represents the spatial downscaling model (i.e., FLUS and Demeter), the superscript i denotes the i^{th} grid cell, and w_i is the geographic area of i^{th} grid cell. Furthermore, we compared the difference both in the spatial pattern and temporal trend of the carbon fluxes under SSP126 and SSP585 in terms of RMSD and Bias. Besides, we also estimated the contribution of future LULCC to GPP, ER, and NEE change by calculating the RMSD and Bias between the simulations using $LULCC_{FLUS}$ and the reference static 2015 land cover:

$$RMSD^{X}_{FLUS,Reference} = \sqrt{\frac{\sum_{1}^{N} w_i (X^{i}_{FLUS} - X^{i}_{Reference})^2}{\sum_{1}^{N} w_i}} \quad (5)$$

$$Bias^{X}_{FLUS,Reference} = \frac{\sum_{1}^{N} w_i (X^{i}_{FLUS} - X^{i}_{Reference})}{\sum_{1}^{N} w_i} \quad (6)$$

where the definition of different symbols is similar to Equation 3 and 4. Note that replacing $LULCC_{FLUS}$ with $LULCC_{Demeter}$ in Eqs. (5-6) derives the similar results, which are not shown in the paper. To compare the relative impact of different LULCC spatial downscaling methods (i.e. FLUS and Demeter) and future LULCC to carbon flux simulations, we further calculated the ratio (Φ_X) of the uncertainty from different LULCC spatial downscaling methods to the contribution of future LULCC to different carbon fluxes X as:

$$\Phi_X = \frac{RMSD^{X}_{FLUS,Demeter}}{RMSD^{X}_{FLUS,Reference}} \quad (7)$$

3 Results

3.1 Uncertain gridded LULCC projections

Results from the downscaling practices with Demeter and FLUS show large spatial difference between $LULCC_{FLUS}$ and $LULCC_{Demeter}$ under both SSP126 and SSP585. Figures S4 and S5 show the spatial patterns of future $LULCC_{Demeter}$ and $LULCC_{FLUS}$ in 2100 under SSP126 and SSP585, as well as the land cover map in 2015 as a reference. The FLUS and Demeter algorithms preserve the total area of each PFT, thus the Bias is relatively small. However, there is large difference in the spatial distributions of the four dominant PFTs over the ABoVE domain from 2020 to 2100, measured by RMSD (Figure 2). In general, the inconsistency between $LULCC_{Demeter}$ and $LULCC_{FLUS}$ rapidly increases in the first few decades and become stable afterwards under both SSP126 and SSP585, and the magnitudes and transition points are different across PFTs and scenarios (Figure 2) following the pattern of the input regional LULCC from GCAM (Figure S3).

The magnitudes are generally larger under SSP126 than those under SSP585 for all the dominant PFTs (Figures 2 and 3). For example, in 2100, the RMSDs between $LULCC_{Demeter}$ and $LULCC_{FLUS}$ are 15.9%, 11.5%, 18.1%, and 18.8%, respectively for the broadleaf deciduous boreal tree, needleleaf evergreen boreal tree, broadleaf deciduous boreal shrub, and C3 arctic grass under SSP126, while those values are 7.5%, 6.2%, 11. 6%, and 10.0%, respectively under SSP585.

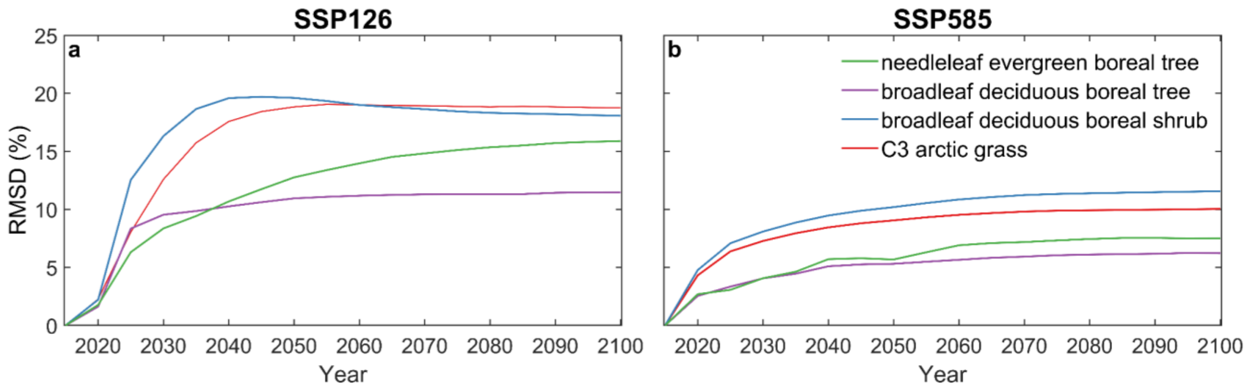

Figure 2. Time series of RMSD between $LULCC_{FLUS}$ and $LULCC_{Demeter}$ for 4 dominant CLM5_PFT types from 2020 to 2100 over the ABOVE domain under (a) SSP126 and (b) SSP585. Green, purple, blue, and red lines represent broadleaf deciduous boreal tree, needleleaf evergreen boreal tree, broadleaf deciduous boreal shrub, and C3 arctic grass separately. A larger RMSD value represents the larger difference between $LULCC_{FLUS}$ and $LULCC_{Demeter}$.

We further compared the areal fraction for four dominant PFTs from $LULCC_{Demeter}$ and $LULCC_{FLUS}$ in 2100 under both SSPs. As shown in Figure 3, the difference between $LULCC_{Demeter}$ and $LULCC_{FLUS}$ is not evenly distributed in the study domain under both SSPs. Under SSP126, compared to Demeter, FLUS prominently distributes up to 95% more needleleaf evergreen boreal trees and less boreal broadleaf deciduous trees in the northwestern ABoVE domain, and more boreal broadleaf deciduous shurbs and less C3 arctic grass in the northern area.

we observed similar spatial patterns in the differences between $LULCC_{FLUS}$ and $LULCC_{Demeter}$ under both SSPs, although with varying magnitudes. Positive values indicate that $LULCC_{FLUS}$ has a greater proportion of the specific PFT compared to $LULCC_{Demeter}$, while negative values indicate that $LULCC_{Demeter}$ has a greater proportion of the PFT compared to $LULCC_{FLUS}$. For needleleaf evergreen boreal trees, the major differences are found in the western region in Alaska. Under both SSPs, in the southeastern regions, the differences show opposite signs under the two SSPs, with negative values ($LULCC_{Demeter}$ is larger) under SSP126 and positive values under SSP585. Southeastern regions show opposite signs of the differences between $LULCC_{FLUS}$ and $LULCC_{Demeter}$ under two scenarios with negative values under SSP126 but positive values under SSP585. For broadleaf deciduous boreal trees, under SSP126, $LULCC_{FLUS}$ indicates more proportion in the southeastern ABoVE domain than $LULCC_{Demeter}$, while under SSP585, $LULCC_{FLUS}$ indicates smaller proportion in the northwestern regions, and up to 50% smaller proportion in the southeastern regions than $LULCC_{Demeter}$. For broadleaf deciduous boreal shrub, $LULCC_{FLUS}$ overall has a larger proportion in the northern regions than $LULCC_{Demeter}$ under SSP126. Under SSP585, $LULCC_{FLUS}$ shows a smaller proportion in the southwestern regions, and a larger value in the western and northern regions than $LULCC_{Demeter}$. For C3 arctic grass, $LULCC_{FLUS}$ shows larger differences from $LULCC_{Demeter}$ with heterogenetic spatial distribution under SSP126, while their difference under SSP585 is smaller, but follows a similar spatial pattern with that under SSP126.

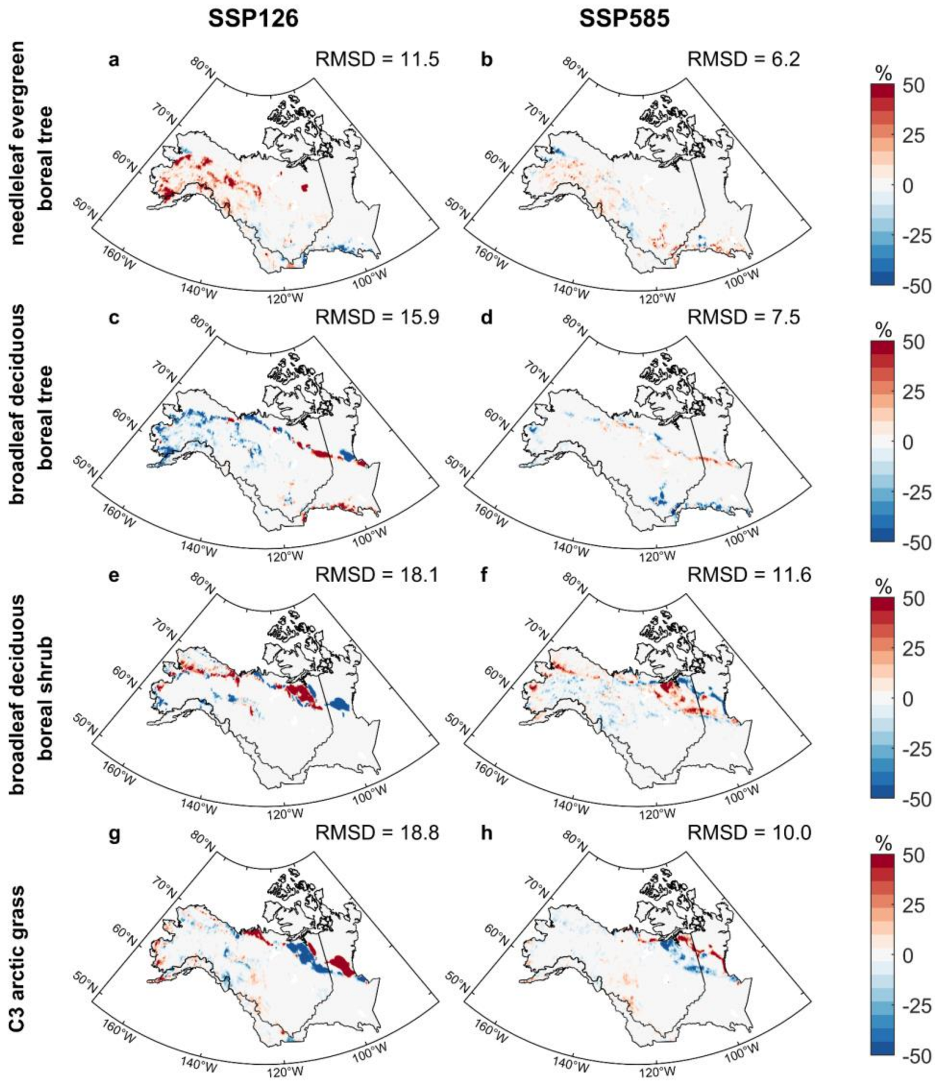

Figure 3. The spatial differences between $LULCC_{FLUS}$ and $LULCC_{Demeter}$ (calculated as $LULCC_{FLUS}$- $LULCC_{Demeter}$) in 2100 for the 4 dominant CLM5_PFT: (a-b) needleleaf evergreen boreal tree, (c-d) broadleaf deciduous boreal tree, (e-f) broadleaf deciduous boreal shrub, and (g-h) C3 arctic grass over the ABoVE domain under (a,c,e,g) SSP126 and (b,d,f,h) SSP585. The corresponding RMSD values (Unit: %) are shown in each panel. Positive values indicate larger PFT fraction by $LULCC_{FLUS}$.

3.2 Impacts of future LULCC uncertainty on terrestrial carbon cycle

Figure 4 shows the differences of CLM5 estimated annual carbon fluxes over the ABoVE domain from 2015 to 2100 between using $LULCC_{FLUS}$ and $LULCC_{Demeter}$ as well as those between using $LULCC_{FLUS}$ and $LULCC_{Reference}$. The RMSD between the results using $LULCC_{FLUS}$ and $LULCC_{Demeter}$ of the estimated carbon fluxes ($RMSD_{FLUS,Demeter}$) increases rapidly with time before 2040, and then becomes stable from 2040 to 2100 under both scenarios. The bias between the estimated carbon fluxes ($Bias_{FLUS,Demeter}$) decreases significantly before 2040 and fluctuates thereafter under SSP126, while such discrepancy is smaller and more stable under SSP585. Such temporal trends are similar to those the differences in the LULCC (Figure 2). By 2100, the $RMSD_{FLUS,Demeter}$ are 120.9, 107.4, and 53.3 gC m^{-2} year^{-1}for GPP, ER and NEE, respectively under SSP126, and are 53.3, 44.9, and 29.7 gC m^{-2} year^{-1}, respectively under SSP585 (Figure 4a,b; Table S1). The Biases in 2100 are -1.7, -1.9, and -0.1 gC m^{-2} year^{-1} under SSP126, and 4.6, -0.6, and -4.0 gC m^{-2} year^{-1} under SSP585 for GPP, ER and NEE, respectively (Figure 4c,d).

Besides, $RMSD_{FLUS,Demeter}$ is comparable to $RMSD_{FLUS,Reference}$. For example, in 2100, the ratios of the uncertainty from different LULCC spatial downscaling methods for GPP, ER, and NEE (Φ_{GPP}, Φ_{ER}, and Φ_{NEE}) are 79.6%, 83.7%, and 79.7%, respectively under SSP126, and are 98.4%, 93.7%, and 97.9% respectively under SSP585. Overall, the $Bias_{FLUS,Demeter}$ is smaller than $Bias_{FLUS,Reference}$ under SSP126, while under SSP585, the $Bias_{FLUS,Demeter}$ is similar to $Bias_{FLUS,Reference}$ and both of them are with small magnitudes.

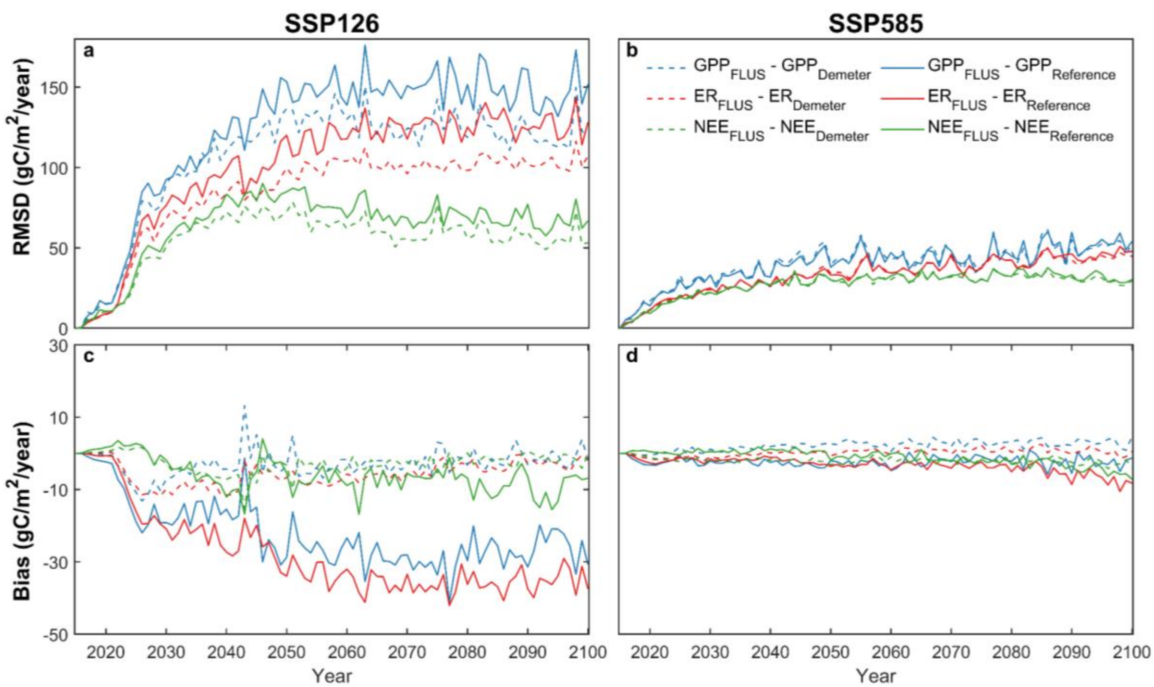

Figure 4. Time series of the RMSD and Bias in (blue) GPP, (red) ER, and (green) NEE, calculated based on the differences (dashed line) between the simulations using $LULCC_{FLUS}$ and $LULCC_{Demeter}$ and the difference (solid line) between the simulations using $LULCC_{FLUS}$ and historical LULCC in 2015, under (a, c) SSP126 and (b, d) SSP585.

We further compared the spatial pattern of the difference between GPP_{FLUS}, ER_{FLUS}, NEE_{FLUS} and $GPP_{Demeter}$, $ER_{Demeter}$, $NEE_{Demeter}$ under both scenarios (Figures 5, S6 and S7). Under SSP126, GPP_{FLUS} is larger in the northwestern regions, but is smaller in the eastern regions than $GPP_{Demeter}$ (Figure 5). The spatial pattern and magnitude of the difference in ER are similar as GPP. For NEE, the spatial pattern of the difference is similar to GPP and ER, but with smaller magnitude and opposite direction except for the southwestern regions. SSP585 shows smaller differences in GPP, ER, and NEE than SSP126 (Figure 5). Under SSP585, the spatial pattern, signs, and magnitudes of the differences in GPP and ER are similar. Positive values can be observed in the southern, central, and western regions, while negative values are present in the southeastern and eastern regions. For NEE, NEE_{FLUS} shows smaller values in the southwestern but larger values in the northwestern and eastern regions than $NEE_{Demeter}$. To better attribute the difference between GPP_{FLUS}, ER_{FLUS}, NEE_{FLUS} and $GPP_{Demeter}$, $ER_{Demeter,}$ $NEE_{Demeter}$ to the uncertainty in gridded LULCC projections, we further investigated the relationship between the difference between $LULCC_{FLUS}$ and $LULCC_{Demeter}$ for each PFT and the difference in GPP, ER, and NEE estimations (Figures 6 and S8). Overall, we found that the grid cells with larger difference between $LULCC_{FLUS}$ and $LULCC_{Demeter}$ correspond to larger differences in all the GPP, ER, and NEE under both SSP126 and SSP585.

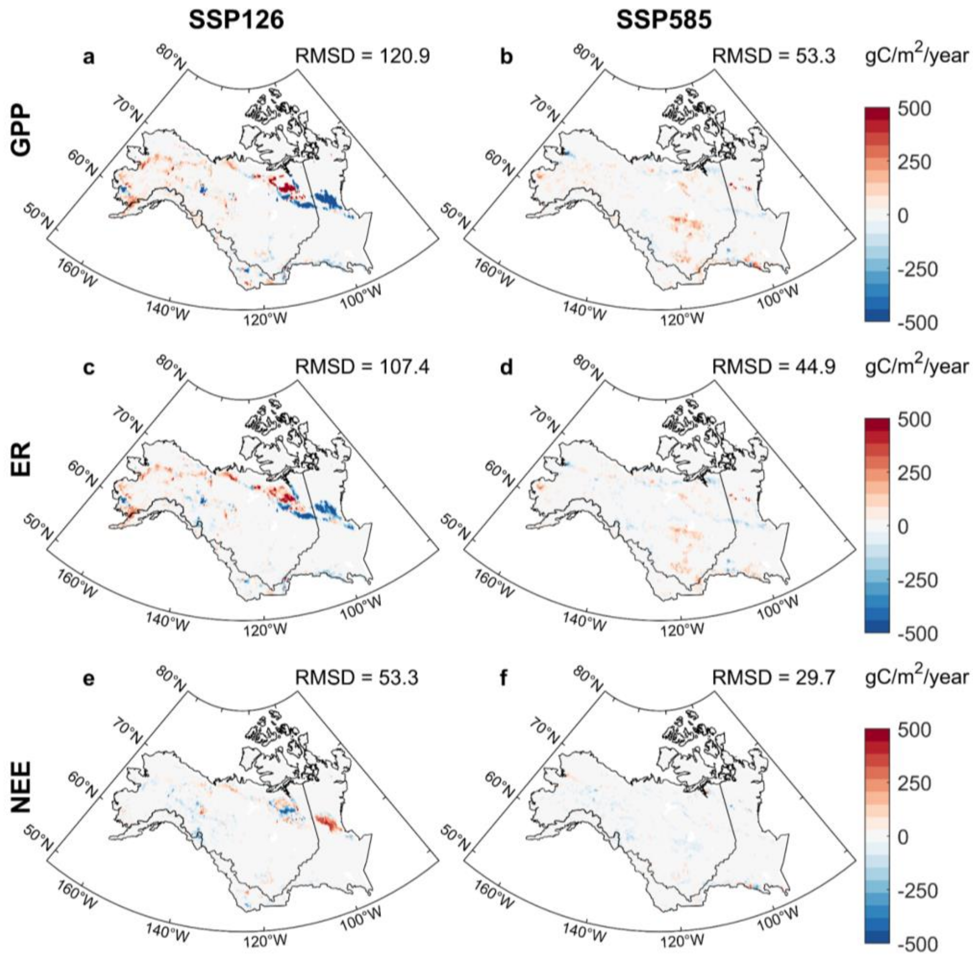

Figure 5. The spatial pattern for the differences of (a-b) GPP_{FLUS} vs $GPP_{Demeter}$, (c-d) ER_{FLUS} vs $ER_{Demeter}$, and (e-f) NEE_{FLUS} vs $NEE_{Demeter}$ in 2100 between CLM5 simulations under (a,c,e) SSP126 and (b,d,f) SSP585. The corresponding $RMSD_{FLUS,Demeter}$ values are shown in each panel.

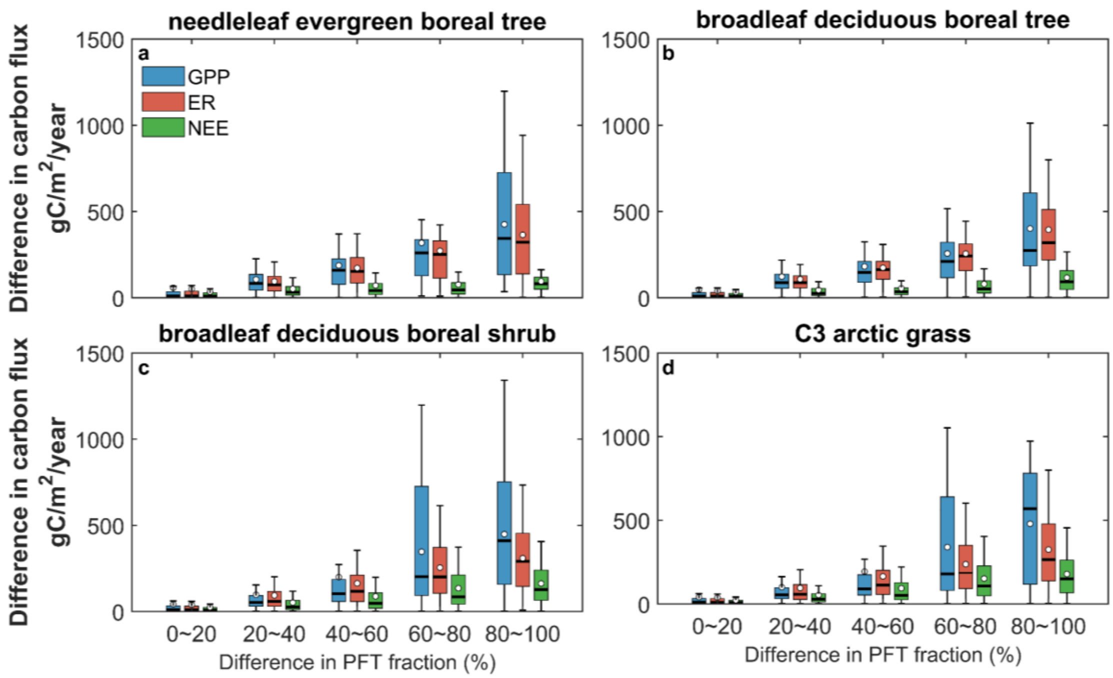

Figure 6. The relationship of the absolute difference in PFT fraction between $LULCC_{FLUS}$ and $LULCC_{Demeter}$ with the corresponding absolute difference in GPP (blue), ER (red), and NEE (green) under SSP126 for 4 PFTs: (a) needleleaf evergreen boreal tree, (b) broadleaf deciduous boreal tree, (c) broadleaf deciduous boreal shrub, and (d) C3 arctic grass.

4 Discussion

Previous studies show that LULCC can cause large uncertainties of carbon cycle estimates that is equivalent to 80% of the net effects of CO_2 and climate(Di Vittorio et al., 2018). There are diverse factors that could contribute to the uncertainties of future gridded LULCC projections. In this study, we focused on quantifying the uncertainty induced by different spatial downscaling methods. Our results indicate that the differences arising from different spatial downscaling methods can be as large as 19% in terms of the RMSD for a single CLM5_PFT type in 2100 in our study region. Furthermore, the impacts of spatial downscaling methods vary with scenarios. The difference between $LULCC_{Demeter}$ and $LULCC_{FLUS}$ increases more rapidly in the first few decades under SSP126 than SSP585 (Figure 2), due to the more rapid increase of regional LULCC projections from GCAM under SSP126. The overall lower $RMSD_{FLUS,Demeter}$ values under SSP585 than under SSP126 is possibly due to the smaller projected regional LULCC from GCAM under SSP585 compared to SSP126 (Figure S5).

Although we observed large spatial discrepancies in projected carbon fluxes due to LULCC differences resulting from different spatial downscaling methods, the discrepancies in projected regional average carbon fluxes are relatively small (Figure 4). Our results are consistent with previous observational-based studies (Dashti et al., 2022), which attributed this phenomenon to the cancellation of opposing signs within a small region with similar climate forcings. Furthermore, the uncertainty of the estimated carbon fluxes from the spatial downscaling methods is generally lower under SSP585 compared to that under SSP126, due to smaller differences between

$LULCC_{Demeter}$ and $LULCC_{FLUS}$ under SSP585 than SSP126. Overall, the impacts of uncertain LULCC on carbon fluxes because of the spatial downscaling process are comparable to the impacts due to future LULCC itself (Figure 4). These stress the importance of considering the uncertainties of the LULCC spatial downscaling methods in carbon cycle projections.

It is important to note that existing spatial downscaling algorithms are inherently different, despite being developed with the same objective. For example, there are several notable differences between Demeter and FLUS that may contribute to the discrepancies between the resulted LULCC product. First, Demeter and FLUS employ different algorithms/methods to determine land types and their respective area proportions in a given grid cell (Li et al., 2017; Liu et al., 2017). Theoretically, Demeter only captures the net change of LULCC (Page et al., 2016; West et al., 2014), while FLUS simulates both gross and net LULCC change. For example, with a given decreased area of shrub from GCAM, we found that Demeter only simulated the shrinkage in shrub under SSP126, while FLUS simulates the shrinkage in most regions and expansions in some parts of the ABoVE domain, reflecting the different assumptions of the two models. Specifically, Demeter assumes that an increasing land type can only encroach a decreasing land type, and a decreasing land type can only be encroached by an increasing land type. These results in that a decreasing land type can only shrink and an increasing land type can only expand or intensify. In contrast, FLUS estimates the combined probabilities for each land type in each grid cell (Li et al., 2017; Liu et al., 2017). making it possible for a decreasing land type to expand in some regions and vice versa. Second, the spatial factors that regulate the downscaling processes in Demeter and FLUS are also different. Demeter has a set of default spatial factors that focus on soil conditions such as soil workability and nutrient availability. In contrast, FLUS typically include the soil condition along with many other spatial factors including climate background (i.e., precipitation and temperature), environmental conditions (e.g., elevation), and socioeconomic factors (i.e., city centers and transportation). In this study, we aim to represent the general performance of both spatial downscaling methods. Thus, we used the default soil conditions for Demeter, and commonly used multiple spatial factors listed in Table 2 for FLUS. Using different spatial factors may also cause the difference in the spatial pattern of the final downscaled LULCC, since these factors are important for estimating the occurrence probability of each land type at a specific grid cell, referred to as probability-of-occurrence in FLUS and suitability index in Demeter (Chen et al., 2019).

Careful consideration of data characteristics, research goals, and future scenarios are critical when selecting a LULCC spatial downscaling method. Additionally, it is important to evaluate the performance and uncertainty of different methods. We recommend selecting the more suitable LULCC spatial downscaling methods based on the research requirements and the unique characteristics of each method. For example, when the land type in the regional projections is different from the land type in the base map, Demeter can be more convenient than FLUS because Demeter can avoid the post-processing steps, e.g., LULCC reclassification. If the study focuses more on the gross LULCC change rather than only the net change, FLUS may be a better choice. Compared to FLUS, Demeter does not consider socioeconomic and environment factors other than soil condition by default, but user can add those factors into Demeter based on their need. It is important to point out there are more spatial downscaling methods beyond the two models discussed in this study, such as Global Land-use Model 2, and Platform for Land-Use and Environmental Model, and thus the uncertainty analyzed here could be possibly even larger than what we show here. Thus, we appeal for attention on the uncertainties of gridded future LULCC data and their applications caused by different spatial downscaling methods, which could be taken into consideration in the future phases of climate model intercomparison project. This study is limited in the ABoVE region, and future studies could expand the scope to other regions and the globe.

5 Conclusions

In this study, we investigated the impact of using different spatial downscaling methods on LULCC projections and their associated impacts on ecosystem carbon fluxes under two global change scenarios. We compared the results from two popular spatial downscaling methods, Demeter and FLUS, using the same regional area projections. Our findings showed that different spatial downscaling methods can result in large differences in the spatial pattern of LULCC and can further induce substantial variations in carbon cycle simulations. Importantly, the uncertainty introduced by spatial downscaling methods is comparable to the uncertainty arising from future LULCC on carbon cycle projections. Additionally, we observed that the uncertainties introduced by spatial downscaling methods under SSP126 were generally larger than those under SSP585, for both gridded LULCC and carbon cycle dynamics. This study highlights the importance of carefully considering the uncertainties associated with spatial downscaling processes and their implications for downstream applications. To address these uncertainties, we recommend choosing the most appropriate spatial downscaling method based on research requirements and unique characteristics of each method.

Acknowledgments

This research was supported by the National Aeronautics and Space Administration (NASA) through Terrestrial Ecology: Arctic Boreal Vulnerability Experiment (ABoVE) grants NNH18ZDA001N (award number 80HQTR19T0055) to Min Chen.

Open Research

MODIS LULCC data are publicly accessible at the Google Earth Engine Platform: https://developers.google.com/earth-engine/datasets/catalog/MODIS_061_MCD12Q1. The future LULCC and carbon flux data is available at https://doi.org/10.6084/m9.figshare.22236652.v4.
The GCAM model can be freely downloaded in https://github.com/JGCRI/gcam-core/releases.
Demeter and FLUS are freely available from https://github.com/JGCRI/demeter, and http://www.geosimulation.cn/FLUS.html, respectively.

References

Alcaraz-Segura, D., Chuvieco, E., Epstein, H. E., Kasischke, E. S., & Trishchenko, A. (2010). Debating the greening vs. browning of the North American boreal forest: Differences between satellite datasets. *Global Change Biology*, *16*(2), 760–770. https://doi.org/10.1111/j.1365-2486.2009.01956.x

Alexander, P., Prestele, R., Verburg, P. H., Arneth, A., Baranzelli, C., Batista e Silva, F., Brown, C., Butler, A., Calvin, K., Dendoncker, N., Doelman, J. C., Dunford, R., Engström, K., Eitelberg, D., Fujimori, S., Harrison, P. A., Hasegawa, T., Havlik, P., Holzhauer, S., … Rounsevell, M. D. A. (2017). Assessing uncertainties in land cover projections. *Global Change Biology*, *23*(2), 767–781. https://doi.org/10.1111/gcb.13447

Bonan, G. B., & Doney, S. C. (2018). Climate, ecosystems, and planetary futures: The challenge to predict life in Earth system models. *Science*, *359*(6375). https://doi.org/10.1126/science.aam8328

Bonan, G. B., Levis, S., Kergoat, L., & Oleson, K. W. (2002). Landscapes as patches of plant functional types: An integrating concept for climate and ecosystem models. *Global Biogeochemical Cycles*, *16*(2), 5-1-5–23. https://doi.org/10.1029/2000gb001360

Bukovsky, M. S., Gao, J., Mearns, L. O., & O'Neill, B. C. (2021). SSP-Based Land-Use Change Scenarios: A Critical Uncertainty in Future Regional Climate Change Projections. *Earth's Future*, *9*(3), 1–18. https://doi.org/10.1029/2020EF001782

Cao, M., Zhu, Y., Quan, J., Zhou, S., Lü, G., & Chen, M. (2010). *Spatial sequential modeling and predication of global land use and land cover changes by integrating a global change assessment model and cellular automata*. 0–1. https://doi.org/10.1029/2019EF001228

Chen, C., Park, T., Wang, X., Piao, S., Xu, B., Chaturvedi, R. K., Fuchs, R., Brovkin, V., Ciais, P., Fensholt, R., Tømmervik, H., Bala, G., Zhu, Z., Nemani, R. R., & Myneni, R. B. (2019). China and India lead in greening of the world through land-use management. *Nature Sustainability*, *2*(2), 122–129. https://doi.org/10.1038/s41893-019-0220-7

Chen, G., Li, X., Liu, X., Chen, Y., Liang, X., Leng, J., Xu, X., Liao, W., Qiu, Y., Wu, Q., & Huang, K. (2020a). Global projections of future urban land expansion under shared socioeconomic pathways. *Nature Communications*, *11*(1), 1–12. https://doi.org/10.1038/s41467-020-14386-x

Chen, M., Vernon, C. R., Graham, N. T., Hejazi, M., Huang, M., Cheng, Y., & Calvin, K. (2020b). Global land use projections for 2015-2100 at 0.05-degree resolution under diverse Shared Socioeconomic Pathways and Representative Concentration Pathways. *Scientific Data*, Submitted. https://doi.org/10.1038/s41597-020-00669-x

Chen, M., Vernon, C. R., Huang, M., Calvin, K. v, Kraucunas, I. P., Northwest, P., Division, G. C., & Northwest, P. (2019). *Calibration and analysis of the uncertainty in downscaling global land use and land cover projections from GCAM using Demeter (v1.0.0)*. 1753–1764.

Cheng, Y., Huang, M., Zhu, B., Bisht, G., Zhou, T., Liu, Y., Song, F., & He, X. (2021). Validation of the Community Land Model Version 5 Over the Contiguous United States (CONUS) Using In Situ and Remote Sensing Data Sets. *Journal of Geophysical Research: Atmospheres*, *126*(5), 1–27. https://doi.org/10.1029/2020JD033539

Dashti, H. *et al.* Underestimation of the impact of land cover change on the biophysical environment of the Arctic and Boreal Region of North America. *Environmental Research Letters* (2022) doi:10.1088/1748-9326/ac8da7.

Di Vittorio, A. V., Mao, J., Shi, X., Chini, L., Hurtt, G., & Collins, W. D. (2018). Quantifying the Effects of Historical Land Cover Conversion Uncertainty on Global Carbon and Climate Estimates. *Geophysical Research Letters*, *45*(2), 974–982. https://doi.org/10.1002/2017GL075124

Doelman, J. C., Stehfest, E., Tabeau, A., van Meijl, H., Lassaletta, L., Gernaat, D. E. H. J., Neumann-Hermans, K., Harmsen, M., Daioglou, V., Biemans, H., van der Sluis, S., & van Vuuren, D. P. (2018). Exploring SSP land-use dynamics using the IMAGE model: Regional and gridded scenarios of land-use change and land-based climate change mitigation. *Global Environmental Change*, *48*(December 2017), 119–135. https://doi.org/10.1016/j.gloenvcha.2017.11.014

Dong, N., You, L., Cai, W., Li, G., & Lin, H. (2018). Land use projections in China under global socioeconomic and emission scenarios: Utilizing a scenario-based land-use change assessment framework. *Global Environmental Change*, *50*(April), 164–177. https://doi.org/10.1016/j.gloenvcha.2018.04.001

Duveiller, G., Hooker, J., & Cescatti, A. (2018). The mark of vegetation change on Earth's surface energy balance. *Nature Communications*, *9*(1). https://doi.org/10.1038/s41467-017-02810-8

Fick, S. E., & Hijmans, R. J. (2017). WorldClim 2: new 1-km spatial resolution climate surfaces for global land areas. *International Journal of Climatology*, *37*(12), 4302–4315. https://doi.org/10.1002/joc.5086

Findell, K. L., Berg, A., Gentine, P., Krasting, J. P., Lintner, B. R., Malyshev, S., Santanello, J. A., & Shevliakova, E. (2017). The impact of anthropogenic land use and land cover change on regional climate extremes. *Nature Communications*, *8*(1), 1–9. https://doi.org/10.1038/s41467-017-01038-w

Friedl, M. A., Sulla-Menashe, D., Tan, B., Schneider, A., Ramankutty, N., Sibley, A., & Huang, X. (2010). MODIS Collection 5 global land cover: Algorithm refinements and characterization of new datasets. *Remote Sensing of Environment*, *114*(1), 168–182. https://doi.org/10.1016/j.rse.2009.08.016

Friedlingstein, P., Jones, M., Sullivan, M. O., & Hauck, J. (2021). *Global Carbon Budget 2021*. *November*. https://doi.org/10.5194/essd-2021-386

Fujimori, S., Hasegawa, T., Ito, A., Takahashi, K., & Masui, T. (2018). Data descriptor: Gridded emissions and land-use data for 2005–2100 under diverse socioeconomic and climate mitigation scenarios. *Scientific Data*, *5*, 1–13. https://doi.org/10.1038/sdata.2018.210

Fujimori, S., Masui, T., & Matsuoka, Y. (2014). Development of a global computable general equilibrium model coupled with detailed energy end-use technology. *Applied Energy*, *128*, 296–306. https://doi.org/10.1016/j.apenergy.2014.04.074

Guivarch, C., Le Gallic, T., Bauer, N., Fragkos, P., Huppmann, D., Jaxa-Rozen, M., Keppo, I., Kriegler, E., Krisztin, T., Marangoni, G., Pye, S., Riahi, K., Schaeffer, R., Tavoni, M., Trutnevyte, E., van Vuuren, D., & Wagner, F. (2022). Using large ensembles of climate change mitigation scenarios for robust insights. *Nature Climate Change*, *12*(5), 428–435. https://doi.org/10.1038/s41558-022-01349-x

Harris, N. L., Gibbs, D. A., Baccini, A., Birdsey, R. A., de Bruin, S., Farina, M., Fatoyinbo, L., Hansen, M. C., Herold, M., Houghton, R. A., Potapov, P. v., Suarez, D. R., Roman-Cuesta, R. M., Saatchi, S. S., Slay, C. M., Turubanova, S. A., & Tyukavina, A. (2021). Global maps of twenty-first century forest carbon fluxes. *Nature Climate Change*, *11*(3), 234–240. https://doi.org/10.1038/s41558-020-00976-6

Hengl, T. (2018). *Global DEM derivatives at 250 m, 1 km and 2 km based on the MERIT DEM [Dataset]*. Zenodo. https://doi.org/https://doi.org/10.5281/zenodo.1447210

Huang, Z., Wu, X., Garcia, A. J., Fik, T. J., & Tatem, A. J. (2013). *An Open-Access Modeled Passenger Flow Matrix for the Global Air Network in 2010*. *8*(5). https://doi.org/10.1371/journal.pone.0064317

Hurtt, G., Chini, L., Sahajpal, R., Frolking, S., Bodirsky, B., Calvin, K., Doelman, J., Fisk, J., Fujimori, S., Goldewijk, K. K., Hasegawa, T., Havlik, P., Heinimann, A., Humpenöder, F., Jungclaus, J., Kaplan, J., Kennedy, J., Kristzin, T., Lawrence, D., … Zhang, X. (2020). Harmonization of Global Land-Use Change and Management for the Period 850–2100 (LUH2) for CMIP6. *Geoscientific Model Development Discussions*, *April*, 1–65. https://doi.org/10.5194/gmd-2019-360

Calvin, K., Bond-Lamberty, B., Clarke, L., Edmonds, J., Eom, J., Hartin, C., Kim, S., Kyle, P., Link, R., Moss, R., McJeon, H., Patel, P., Smith, S., Waldhoff, S., & Wise, M. (2017). The SSP4: A world of deepening inequality. *Global Environmental Change*, *42*, 284–296. https://doi.org/10.1016/j.gloenvcha.2016.06.010

Calvin, K., Patel, P., Clarke, L., Asrar, G., Bond-lamberty, B., Cui, R. Y., Vittorio, A. di, Dorheim, K., Edmonds, J., Hartin, C., Hejazi, M., Horowitz, R., Iyer, G., Kyle, P., Kim, S., Link, R., Mcjeon, H., Smith, S. J., Snyder, A., … Calvin, C. K. (2019). *GCAM v5 . 1 : representing the linkages between energy , water , land , climate , and economic systems*. 677–698.

Lawrence, D. M., Fisher, R. A., Koven, C. D., Oleson, K. W., Swenson, S. C., Bonan, G., Collier, N., Ghimire, B., van Kampenhout, L., Kennedy, D., Kluzek, E., Lawrence, P. J., Li, F., Li, H., Lombardozzi, D., Riley, W. J., Sacks, W. J., Shi, M., Vertenstein, M., … Zeng, X. (2019). The Community Land Model Version 5: Description of New Features, Benchmarking, and Impact of Forcing Uncertainty. *Journal of Advances in Modeling Earth Systems*, *11*(12), 4245–4287. https://doi.org/10.1029/2018MS001583

Li, X., Chen, G., Liu, X., Liang, X., Wang, S., Chen, Y., Pei, F., & Xu, X. (2017). A New Global Land-Use and Land-Cover Change Product at a 1-km Resolution for 2010 to 2100 Based on Human–Environment Interactions. *Annals of the American Association of Geographers*, *107*(5), 1040–1059. https://doi.org/10.1080/24694452.2017.1303357

Liao, W., Liu, X., Xu, X., Chen, G., Liang, X., Zhang, H., & Li, X. (2020). Projections of land use changes under the plant functional type classification in different SSP-RCP scenarios in China. *Science Bulletin*, *xxxx*. https://doi.org/10.1016/j.scib.2020.07.014

Liu, J., Wennberg, P. O., Parazoo, N. C., Yin, Y., & Frankenberg, C. (2020). Observational Constraints on the Response of High-Latitude Northern Forests to Warming. *AGU Advances*, *1*(4). https://doi.org/10.1029/2020av000228

Liu, X., Liang, X., Li, X., Xu, X., Ou, J., Chen, Y., Li, S., Wang, S., & Pei, F. (2017a). A future land use simulation model (FLUS) for simulating multiple land use scenarios by coupling human and natural effects. *Landscape and Urban Planning*, *168*(November), 94–116. https://doi.org/10.1016/j.landurbplan.2017.09.019

Luo, M., Hu, G., Chen, G., Liu, X., Hou, H., & Li, X. (2022). 1 km land use/land cover change of China under comprehensive socioeconomic and climate scenarios for 2020–2100. *Scientific Data*, *9*(1), 1–13. https://doi.org/10.1038/s41597-022-01204-w

Ma, L., Hurtt, G., Chini, L., Sahajpal, R., Pongratz, J., Frolking, S., Stehfest, E., Klein Goldewijk, K., O' Leary, D., & Doelman, J. (2019). Global Transition Rules for Translating Land-use Change (LUH2) To Land-cover Change for CMIP6 using GLM2. *Geoscientific Model Development*, *July*, 1–30. https://doi.org/10.5194/gmd-2019-146-supplement

Mekonnen, Z. A., Riley, W. J., Berner, L. T., Bouskill, N. J., Torn, M. S., Iwahana, G., Breen, A. L., Myers-Smith, I. H., Criado, M. G., Liu, Y., Euskirchen, E. S., Goetz, S. J., Mack, M. C., & Grant, R. F. (2021). Arctic tundra shrubification: a review of mechanisms and impacts on ecosystem carbon balance. In *Environmental Research Letters* (Vol. 16, Issue 5). IOP Publishing Ltd. https://doi.org/10.1088/1748-9326/abf28b

Page, Y. Le, West, T. O., Link, R., & Patel, P. (2016). *Downscaling land use and land cover from the Global Change Assessment Model for coupling with Earth system models*. 3055–3069. https://doi.org/10.5194/gmd-9-3055-2016

Pastick, N. J., Jorgenson, M. T., Goetz, S. J., Jones, B. M., Wylie, B. K., Minsley, B. J., Genet, H., Knight, J. F., Swanson, D. K., & Jorgenson, J. C. (2019). Spatiotemporal remote sensing of ecosystem change and causation across Alaska. *Global Change Biology*, *25*(3), 1171–1189. https://doi.org/10.1111/gcb.14279

Popp, A., Humpenöder, F., Weindl, I., Bodirsky, B. L., Bonsch, M., Lotze-Campen, H., Müller, C., Biewald, A., Rolinski, S., Stevanovic, M., & Dietrich, J. P. (2014). Land-use protection for climate change mitigation. *Nature Climate Change*, *4*(12), 1095–1098. https://doi.org/10.1038/nclimate2444

Riahi, K., Vuuren, D. P. Van, Kriegler, E., Edmonds, J., Neill, B. C. O., Fujimori, S., Bauer, N., Calvin, K., Dellink, R., Fricko, O., Lutz, W., Popp, A., Crespo, J., Kc, S., Leimbach, M., Jiang, L., Kram, T., Rao, S., Emmerling, J., … Tavoni, M. (2017). *The Shared Socioeconomic Pathways and their energy , land use , and greenhouse gas emissions implications : An overview*. *42*, 153–168. https://doi.org/10.1016/j.gloenvcha.2016.05.009

Semenchuk, P., Plutzar, C., Kastner, T., Matej, S., Bidoglio, G., Erb, K. H., Essl, F., Haberl, H., Wessely, J., Krausmann, F., & Dullinger, S. (2022). Relative effects of land conversion and land-use intensity on terrestrial vertebrate diversity. *Nature Communications*, *13*(1). https://doi.org/10.1038/s41467-022-28245-4

Song, X. P., Hansen, M. C., Stehman, S. V., Potapov, P. V., Tyukavina, A., Vermote, E. F., & Townshend, J. R. (2018). Global land change from 1982 to 2016. *Nature*, *560*(7720), 639–643. https://doi.org/10.1038/s41586-018-0411-9

Sterling, S. M., Ducharne, A., & Polcher, J. (2013). The impact of global land-cover change on the terrestrial water cycle. *Nature Climate Change*, *3*(4), 385–390. https://doi.org/10.1038/nclimate1690

Vernon, C. R., Page, Y. Le, Chen, M., Huang, M., Calvin, K. V, Kraucunas, P., & Braun, C. J. (2018). Demeter – A Land Use and Land Cover Change Disaggregation Model. *Journal of Open Research Software*, *6*(1), 15. https://doi.org/http://doi.org/10.5334/jors.208

West, T. O., Brandt, C. C., Baskaran, L. M., Hellwinckel, C. M., Mueller, R., Bernacchi, C. J., Bandaru, V., Yang, B., Wilson, B. S., Marland, G., Nelson, R. G., De La Torre Ugarte, D. G., & Post, W. M. (2010). Cropland carbon fluxes in the United States: Increasing geospatial resolution of inventory-based carbon accounting. *Ecological Applications*, *20*(4), 1074–1086. https://doi.org/10.1890/08-2352.1

West, T. O., Page, Y. Le, Huang, M., Wolf, J., & Thomson, A. M. (2014). *Downscaling global land cover projections from an integrated assessment model for use in regional analyses : results and evaluation for the US from 2005 to 2095*. https://doi.org/10.1088/1748-9326/9/6/064004

Wu, W., Hasegawa, T., Ohashi, H., Hanasaki, N., Liu, J., Matsui, T., Fujimori, S., Masui, T., & Takahashi, K. (2019). Global advanced bioenergy potential under environmental protection policies and societal transformation measures. *GCB Bioenergy*, *11*(9), 1041–1055. https://doi.org/10.1111/gcbb.12614

Uncertain spatial pattern of future land use and land cover change and its impacts on terrestrial carbon cycle over the Arctic–Boreal region of North America

Meng Luo[1], Fa Li[1], Dalei Hao[2], Qing Zhu[3], Hamid Dashti[1], Min Chen[1]

[1]Department of Forest and Wildlife Ecology, University of Wisconsin-Madison, Madison, WI, USA.

[2]Atmospheric Sciences and Global Change Division, Pacific Northwest National Laboratory, Richland, WA, USA

[3]Climate and Ecosystem Sciences Division, Lawrence Berkeley National Laboratory, Berkeley, CA, USA.

Corresponding author: Min Chen (mchen392@wisc.edu)

Key Points:

- We identified a traditionally ignored source of uncertainty in model projected carbon cycle from the future land use and land cover change (LULCC) data.
- Spatial downscaling is a necessary step for generating gridded LULCC data, but different downscaling methods may lead to results with large spatial differences.
- The impacts of using different spatial downscaling methods are more than 79% of the contributions of future LULCC to carbon cycle projections in 2100.

Abstract

Land use and land cover change (LULCC) represents a key process of human-Earth system interaction and has profound impacts on terrestrial ecosystem carbon cycling. As a key input for ecosystem models, future gridded LULCC data is typically spatially downscaled from regional LULCC projections by integrated assessment models, such as the Global Change Analysis Model (GCAM). The uncertainty associated with the different spatial downscaling methods and its impacts on the subsequent model projections have been historically ignored and rarely examined. This study investigated this problem using two representative spatial downscaling methods and focused on their impacts on the carbon cycle over the Arctic-Boreal Vulnerability Experiment (ABoVE) domain where extensive LULCC is expected. Specifically, we used the Future Land Use Simulation model (FLUS) and the Demeter model to generate 0.25-degree gridded LULCC data (i.e., $LULCC_{FLUS}$ and $LULCC_{Demeter}$, respectively) with the same input of regional LULCC projections from GCAM, under both the low (i.e., SSP126) and high (i.e., SSP585) greenhouse gas emission scenarios. The two sets of downscaled LULCC were used to drive the Community Land Model version 5 (CLM5) to prognostically simulate the terrestrial carbon cycle dynamics over the 21st century. The results suggest large spatial-temporal differences between $LULCC_{FLUS}$ and $LULCC_{Demeter}$, and the spatial distributions of the needleleaf evergreen boreal tree, broadleaf deciduous boreal tree, broadleaf deciduous boreal shrub, and C3 arctic grass are particularly different under both SSP126 and SSP585. The LULCC differences further lead to large discrepancies in the spatial patterns of projected gross primary productivity, ecosystem respiration, and net ecosystem exchange, which are more than 79% of the contributions of future LULCC in 2100. Besides, the difference for LULCC and carbon flux under SSP126 is generally larger than those under SSP585. This study highlights the importance of considering the uncertainties induced by the spatial downscaling process in future LULCC projections and carbon cycle simulations.

Plain Language Summary

Land use and land cover change (LULCC) affects the carbon cycle in ecosystems. To predict future LULCC and carbon cycle changes, scientists use spatial downscaling methods to create detailed LULCC maps. However, different methods can lead to different results and can impact carbon cycle projections. Our study found that using different spatial downscaling methods can lead to a large portion of the uncertainty in future LULCC and carbon cycle projections over the Arctic-Boreal region. It is important to consider these uncertainties when studying future changes in land use and carbon cycling.

1 Introduction

Land use and land cover change (LULCC) represents a key human impact on the Earth system (Chen et al., 2019). It has crucial impact on many important ecological, biophysical, biogeochemical and climatic processes such as biodiversity (Semenchuk et al., 2022), energy balance (Duveiller et al., 2018; Dashti et al., 2022), carbon and water cycle (Harris et al., 2021; Friedlingstein et al., 2021; Sterling et al., 2013), and climate extremes (Findell et al., 2017). Substantial LULCC has occurred in the past several decades (Song et al., 2018; J. Liu et al., 2020) and is expected to continue in the future (Doelman et al., 2018; Friedlingstein et al., 2021; Chen et al., 2020b; Bukovsky et al., 2021). Under global climate change, the Arctic-Boreal Vulnerability Experiment (ABoVE) domain is a vulnerable hotspot region, due to the amplified warming (Liu et al., 2020), and has been used as a key representative region to understand the changes in the whole Arctic. Extensive LULCC has been observed by satellites in this region (Alcaraz-Segura et al., 2010), such as the shrub expansion and forest cover change (Alcaraz-Segura et al., 2010; Pastick et al., 2019). Previous study found the historical LULCC over this region has large impacts on carbon cycle (Mekonnen et al., 2021). Projecting and understanding how future LULCC will evolve and its ecological impacts over the ABoVE domain are of vital importance for making mitigation and adaptation strategies and sustainable management of ecosystems in this region and the whole high-latitude area.

Gridded LULCC projection is essential to analyze the spatial patterns of LULCC and to understand the impact of LULCC on important ecosystem services, e.g., carbon sequestration, in the future. Integrated Assessment Models (IAMs) are commonly used to project future LULCC under diverse global change scenarios. However, these IAM projections are usually under large political, economic, or geographical region level, and spatial downscaling is a necessary step to obtain a spatially explicit LULCC data (i.e. gridded LULCC) from the IAM projections. Recent studies have investigated the large uncertainties in the future gridded LULCC due to the difference in interpretations of narratives, model assumptions, and structure of IAMs (Riahi et al., 2017; Guivarch et al., 2022) as well as the difference in spatial resolution (Alexander et al., 2017) and LULCC definitions (Chen et al., 2020b). For instance, the computable-general equilibrium models such as the Global Change Analysis Model (GCAM) (Calvin et al., 2017, 2019), have a smaller area of projected cropland in the last half of the 21st century than the partial equilibrium models (Alexander et al., 2017) like the Model of Agricultural Production and its Impact on the Environment (MAgPIE; Popp et al., 2014), despite both models are among the major IAMs in the world. These uncertainties could propagate and result in large uncertainties in the following analyses of LULCC impacts, such as the quantification of critically important terrestrial ecosystem carbon cycle (Di Vittorio et al., 2018) in Earth System Models.

However, as a key step of generating gridded LULCC data, spatial downscaling also has large uncertainties that, to the best of our knowledge, have received limited attention. The difference in the downscaled LULCC due to different spatial downscaling methods remains underexplored and it is unclear how big the difference could be. Several spatial downscaling methods, e.g., Demeter (Chen et al., 2019; Chen et al., 2020b; Vernon et al., 2018), FLUS (Dong et al., 2018; Cao et al., 2010; Luo et al., 2022), Global Land-use Model 2 (Ma et al., 2019; Hurtt et al., 2020), and Platform for Land-Use and Environmental Model (Wu et al., 2019; Fujimori et al., 2018), have been widely used to disaggregate regional LULCC projections from IAMs. Although these models/methods can take in the same regional LULCC projections from the same IAM, their mechanisms of disaggregating the areal projection into grid levels are different. For instance, Demeter uses the proximal relationships defined by kernel density probabilities to process the intensification and expansion of LULCC (Vernon et al., 2018), while FLUS combines the artificial neural networks (ANN) and the mechanisms of cellular automata (CA) (Liu et al., 2017) to couple both human-related and natural environmental effects and consider the interactions and competition among different land types. These differences are expected to cause diverse spatial patterns of future LULCC projections, which could further influence the subsequent projections of terrestrial ecosystem carbon fluxes, such as the gross primary productivity (GPP), ecosystem respiration (ER), and their difference net ecosystem exchange (NEE; NEE=ER-GPP).

This study focuses on the future LULCC and carbon fluxes in the ABoVE domain under two Shared Socioeconomic Pathways (SSPs), i.e., SSP126 and SSP585). We aim to answer two questions: 1) how much uncertainty of the spatial pattern of LULCC could be caused by different spatial downscaling methods and 2) what are the impacts on the subsequent projections of ecosystem carbon fluxes with the uncertain downscaled LULCC? For this purpose, we used two different spatial downscaling methods (i.e., Demeter and FLUS) to generate 0.25-degree gridded LULCC data with the same LULCC classification and definitions based on the same regional projections from GCAM from 2015 to 2100. We then used the Community Land Model version 5 (CLM5) to simulate the carbon fluxes driven by the gridded LULCC data produced by Demeter and FLUS, respectively. Thereby, we quantified the differences of gridded LULCC generated by Demeter and FLUS and their impacts on future GPP, ER, and NEE projections.

2 Materials and Methods

2.1 Demeter and FLUS

Demeter is a LULCC spatial disaggregation model developed as part of the GCAM software ecosystem and could be extended to other IAMs (Vernon et al., 2018). It uses an intensification and expansion strategy (Page et al., 2016; West et al., 2010) to perform the spatial downscaling, following a series of user-defined rules. Specifically, the treatment order defines final land type is downscaled first. Transition priorities define what type of land swaps are favored. Spatial constraints, e.g., kernel density, measure the probability density of a land type around a given grid cell. The soil workability and nutrient availability help to indicate suitability for agriculture. Detailed algorithms and optimization procedures can refer to the previous studies (Chen et al., 2019; Vernon et al., 2018).

FLUS is a CA-based model which can be used to explore nonlinear relationships between the complex spatial factors and multiple land types (Liu et al., 2017; Liao et al., 2020). FLUS first estimates the probability of occurrence for each LULCC on each grid cell based on ANN. Then FLUS accounts for the competition and interactions among different land types and carries out the land allocation by combining the probability-of-occurrence, user-defined conversion cost, neighborhood condition, and competition among different land types and the mechanisms of CA, self-adaptive inertia, and competition mechanism. During this stage, the land type with a higher probability-of-occurrence is more likely to be predicted as the target land type, while those with a relatively lower probability-of-occurrence can still be possibly converted based on the roulette selection mechanism.

2.2 Data preparation for LULCC spatial downscaling

We used the regional LULCC projections under both the low (i.e., SSP126) and high (i.e., SSP585) emission scenarios derived from GCAM (Chen et al., 2020b) as the input for the spatial downscaling (Figure S1). SSP126 describes a sustainability scenario pathway with an increase of global mean temperature by 1.5°C to 2 °C compared to the pre-industrial level by the end of the 21st century. SSP585 describes a world that widely uses fossil-fuels and the global mean temperature increase by about 4.4 °C by the end of the 21st century. Under both scenarios, GCAM projects LULCC at 5-year time step over 2015-2100 in 384 regions globally, ten of which locate in the ABoVE domain (Figure 1).

Both Demeter and FLUS require a gridded land cover map at the target spatial resolution as the reference for their spatial disaggregation, and here we used the year 2015 land cover map at a spatial resolution of 500m provided by the MODerate resolution Imaging Spectroradiometer (MODIS) land cover product (MCD12Q1 C6). Specifically, we used the Plant Functional Types

(PFT) classification in MCD12Q1 (hereafter referred to MODIS_PFT) (Friedl et al., 2010), which classifies the global land surface into 11 types. However, MODIS_PFT is different from the land classification system of GCAM and that of the downstream land surface model CLM5 (CLM5_PFT) (Lawrence et al., 2019). Therefore, a few reclassification steps (Figure S2) were applied to harmonize the differences, following a similar strategy used in the previous studies (Chen et al., 2020b; Luo et al., 2022).

Specifically, Demeter allows inconsistent classification systems among the input (GCAM), reference map (MODIS_PFT) and the target (CLM_PFT). The spatial downscaling can be performed with Demeter once the links among the three classification systems are defined. In contrast, the design of FLUS requires an identical land cover type classification system across input, reference and target. Therefore, we first consolidated both GCAM and MODIS_PFT type into 7 broad types and built a reclassification scheme (Table 1) for the harmonization. For Demeter, we reclassified the 11-type 500m MODIS land cover map into 18 CLM5_PFT types (Figure 1) based on the climate-based rules as described in Bonan et al. (2002), using the WorldClim V2 monthly climatological temperature and precipitation data (Fick & Hijmans, 2017). The reclassified 500 m MODIS data was then aggregated to 0.25 degree to be used as the reference map for Demeter downscaling in this study. For FLUS, we reclassified the MODIS reference land cover map to a new reference map with the 7 broad types. Spatial downscaling with FLUS thus generated LULCC data in the same 7 broad types, and we finally mapped the 7 broad types into the 18 CLM5_PFT types by using a similar strategy in a previous study (Chen et al., 2020a) that iteratively assign the new label of the nearest neighbor for each map grid in each year. It must be noted that the differences in these preprocessing steps are also an inherent uncertainty source of the gridded LULCC products while using different spatial downscaling models.

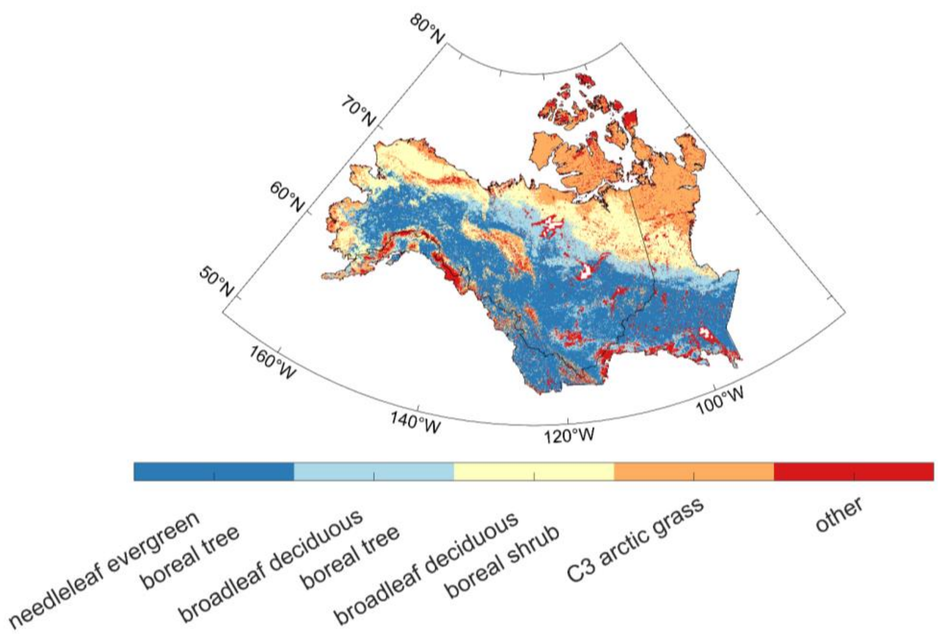

Figure 1. The spatial distribution of LULCC over the ABoVE domain in 2015. Different colors represent different CLM5_PFT types**.**

In addition, due to the errors in the geographical data (Chen et al., 2020b; Luo et al., 2022) used in GCAM, the geographical areas between GCAM regional projections and MODIS reference map are not consistent and also need to be harmonized. Specifically, for Demeter, we used the Eq. (1) to harmonize the LULCC projections (Chen et al., 2020b):

$$A_{GLT,u,H}(t) = \begin{cases} A_{BLT,u,B}(t) \times \frac{A_{GLT,u,G}(t)}{A_{BLT,u,G}(t)} & t = 2015 \\ A_{GLT,u,H}(t-1) \times \frac{A_{GLT,u,G}(t)}{A_{GLT,u,G}(t-1)} & 2020 \leq t \leq 2100 \end{cases} \quad (1)$$

where $A_{GLT,u,H}(t)$ is the harmonized area in region *u* in year t for each GCAM type (GLT). $A_{BLT,u,B}(t)$ is the area in region *u* in the reference map in year *t* for each broad type (BLT). $A_{GLT,u,G}(t)$ is the area in region *u* from GCAM projections in year *t* for each GLT. $A_{BLT,u,G}(t)$ is the area in region *u* from GCAM projection for each BLT in year *t*.

Considering that FLUS uses the broad land types during the spatial downscaling process, we used Eq. (2) to harmonize the regional area between GCAM and the reference map (Luo et al., 2022):

$$A_{BLT,u,H}(t) = \begin{cases} A_{BLT,u,B}(t) & t = 2015 \\ A_{BLT,u,H}(t-1) \times \frac{A_{BLT,u,G}(t)}{A_{BLT,u,G}(t-1)} & 2020 \leq t \leq 2100 \end{cases} \quad (2)$$

where $A_{BLT,u,H}$ is the harmonized area in region *u* for each BLT. Such area harmonization for Demeter and FLUS makes sure that the input LULCC projections are adjusted to match the reference map and be consistent in our Demeter and FLUS experiments.

Table 1. *LULCC reclassification scheme for GCAM type, Broad type, MODIS_PFT, and CLM5_PFT.*

GCAM type	Broad type	MODIS_PFT	CLM5_PFT
RockIceDesert	Barren	Barren	Barren
biomass-grass_IRR, biomass-grass_RFD, biomass-tree_IRR, biomass-tree_RFD, Corn_IRR, Corn_RFD, FiberCrop_IRR, FiberCrop_RFD, FodderGrass_IRR, FodderGrass_RFD, FodderHerb_IRR, FodderHerb_RFD, MiscCrop_IRR, MiscCrop_RFD, OilCrop_IRR, OilCrop_RFD, OtherArableLand, OtherGrain_IRR, OtherGrain_RFD, Root-Tuber_IRR, Root-Tuber_RFD, SugarCrop_IRR, SugarCrop_RFD, Wheat_IRR, Wheat_RFD,	Cropland	Cereal Croplands, Broadleaf Croplands	Crop
Forest, Unmanaged Forest	Forest	Evergreen Needleleaf Trees	Needleleaf evergreen temperate tree, Needleleaf evergreen boreal tree
		Deciduous Needleleaf Trees	Needleleaf deciduous boreal tree
		Evergreen Broadleaf Trees	Broadleaf evergreen tropical tree, Broadleaf evergreen temperate tree
		Deciduous Broadleaf Trees	Broadleaf deciduous tropical tree, Broadleaf deciduous temperate tree, Broadleaf deciduous boreal tree
Grassland, Tundra, Pasture, Unmanaged Pasture,	Grass	Grass	C3 arctic grass, C3 non-arctic grass, C4 grass,
Shrubland	Shrub	Shrub	Broadleaf evergreen temperate shrub, Broadleaf deciduous temperate shrub, Broadleaf deciduous boreal shrub
UrbanLand	Urban	Urban and Built-up Lands	Urban
None	Water	Water Bodies	Water

2.3 Generating gridded LULCC with Demeter and FLUS

We used two spatial downscaling methods (i.e., Demeter and FLUS) to generate the gridded LULCC data at a 5-year interval from 2015 to 2100, in line with GCAM (Figure S1). For Demeter, key parameters such as the optimal value of the ratio of allocating LULCC as intensification, and threshold percentage of suitable grid cells to accept extensified LULCC allocation used were set as the calibrated values in Chen et al. (2020b). We also used the same treatment order of each land type, and transition priority as that in Chen et al. (2020b). These rules and constraints, together with kernel density probabilities, were used to conduct the intensification and expansion to apply the projected future LULCC allocation. For FLUS, to estimate the probability of occurrence, we first collected the base map in 2015 (see Section 2.2) and 9 spatial factors (shown in Table 2), which reflect different heterogeneous characteristics (i.e., climate, topography, transportation, etc.) related to LULCC (Chen et al., 2020a; Liu et al., 2017; Luo et al., 2022) as the training data for ANN. All these spatial factors were reprojected into 500 m spatial resolution. Other parameters including sampling method, sample rate, and hidden layer were set based on Luo et al. (2022). During the allocation stage, we set the user-defined conversion cost, neighborhood condition, and competition based on the optimal values in Luo et al. (2022). Based on the based map and the abovementioned parameter configuration, we used FLUS to produce 500 m LULCC dataset in the ABoVE domain from 2015 to 2100.

FLUS outputs LULCC at a spatial resolution of 500 m. We aggregated the FLUS outputs into the same resolution as Demeter (i.e., 0.25 degree), and both of them can be used as CLM5. We hereafter refer to two gridded LULCC data produced by Demeter and FLUS as $LULCC_{Demeter}$ and $LULCC_{FLUS}$, respectively. Note that the two datasets are identical in the starting year 2015, since both Demeter and FLUS kept their downscaled maps the same as the reference map in the starting year.

2.4 Projecting future carbon cycle

We used CLM5 to prognostically project the future GPP, ER, and NEE under the two scenarios driven by $LULCC_{Demeter}$ and $LULCC_{FLUS}$, respectively (Figure S1). CLM5 is the land component of the Community Earth System Model version 2.0, which is a state-of-the-art land surface model that mechanistically simulate the biogeophysical, biogeochemical, and ecological processes in the terrestrial environment simultaneously and is an effective tool to quantify impact of LULCC on carbon cycle over a wide range of spatial and temporal scales (Bonan & Doney, 2018; Cheng et al., 2021). Compared to the previous version, CLM5 generally has improved performance in capturing the dynamics of ecosystem carbon cycle (Lawrence et al., 2019).

Specifically, we carried out the CLM5 simulations with biogeochemistry mode for 200 years in an "accelerated decomposition" mode, and subsequently for 400 years in regular spin-up mode by cycling through 2000-2014 to get the steady initial conditions. For the future projections from 2015-2100, we first linearly interpolated the 5-year interval $LULCC_{Demeter}$ and $LULCC_{FLUS}$ into 1-year interval. Then we carried out the future CLM5 simulations using the yearly $LULCC_{Demeter}$, $LULCC_{FLUS}$ from 2015-2100 under both SSP126 and SSP585, respectively. In order to evaluate the impacts of LULCC on future ecosystem carbon cycle, we also carried out another reference 2015-2100 CLM5 simulation with a static land cover in 2015. We hereafter refer to the three sets of GPP, ER, and NEE projections using $LULCC_{Demeter}$, $LULCC_{FLUS}$ and historical LULCC in 2015 as 1) GPP_{FLUS}, ER_{FLUS}, NEE_{FLUS}, 2) $GPP_{Demeter}$, $ER_{Demeter}$, $NEE_{Demeter}$, and 3) $GPP_{Reference}$, $ER_{Reference}$, $NEE_{Reference}$. During the spin-up and future simulations, we used the meteorological forcing data of the Geophysical Fluid Dynamics Laboratory (GFDL) from the standard Inter-Sectoral Impact Model Intercomparison Project phase 3b (ISIMIP3b)(https://www.isimip.org/protocol/3/). The original daily GFDL forcing data was downscaled to 6-hourly based on the diurnal cycle from the Climatic Research Unit - NCEP (CRUNCEP) datasets.

Table 2. *Specifications of the 9 spatial factors used in FLUS during the spatial downscaling process.*

Spatial factor	Period	Spatial resolution	Data source
Annual mean temperature Annual precipitation	Climatological (1970-2000)	0.5'	WorldClim v2.0 (http://www.worldclim.org/)
DEM Slope	1996	1 km	Hengl (2018)
Distance to water	2015	500 m	MODIS PFT (Friedl et al., 2010)
Distance to main roads Distance to highway	1980-2010	500 m	Global Roads Open Access Data Set (gROADS) (https://sedac.ciesin.columbia.edu/data/set/groads-global-roads-open-access-v1/)
Distance to airports	2010	500 m	Huang et al. (2013)Click or tap here to enter text.
Distance to urban centers	2014	500 m	United Nations, Department of Economic Social Affairs, Population Division

2.5 Evaluating the uncertainties of the gridded LULCC dynamics and their impact on future ecosystem carbon cycle

To evaluate the uncertainties induced by two different spatial downscaling methods, we compared the spatial and temporal patterns of $LULCC_{Demeter}$ and $LULCC_{FLUS}$ and the resulted carbon fluxes under SSP126 and SSP585, separately. Here the uncertainties are quantified as the difference in gridded LULCC and carbon fluxes caused by using different LULCC spatial downscaling methods. We calculated the Root Mean Square Deviation (RMSD) and Bias for each CLM5_PFT type between $LULCC_{Demeter}$ and $LULCC_{FLUS}$ to quantify the spatial differences at each year:

$$RMSD_{FLUS,Demeter}^{X} = \sqrt{\frac{\sum_1^N w_i (X_{FLUS}^i - X_{Demeter}^i)^2}{\sum_1^N w_i}} \quad (3)$$

$$Bias_{FLUS,Demeter}^{X} = \frac{\sum_1^N w_i (X_{FLUS}^i - X_{Demeter}^i)}{\sum_1^N w_i} \quad (4)$$

where N is the number of grid cells, X represents the variables of interest (e.g., fraction of each CLM5_PFT type, GPP, ER, or NEE), the subscript of X represents the spatial downscaling model (i.e., FLUS and Demeter), the superscript i denotes the i^{th} grid cell, and w_i is the geographic area of i^{th} grid cell. Furthermore, we compared the difference both in the spatial pattern and temporal trend of the carbon fluxes under SSP126 and SSP585 in terms of RMSD and Bias. Besides, we also estimated the contribution of future LULCC to GPP, ER, and NEE change by calculating the RMSD and Bias between the simulations using $LULCC_{FLUS}$ and the reference static 2015 land cover:

$$RMSD^{X}_{FLUS,Reference} = \sqrt{\frac{\sum_{1}^{N} w_i (X^{i}_{FLUS} - X^{i}_{Reference})^2}{\sum_{1}^{N} w_i}} \quad (5)$$

$$Bias^{X}_{FLUS,Reference} = \frac{\sum_{1}^{N} w_i (X^{i}_{FLUS} - X^{i}_{Reference})}{\sum_{1}^{N} w_i} \quad (6)$$

where the definition of different symbols is similar to Equation 3 and 4. Note that replacing $LULCC_{FLUS}$ with $LULCC_{Demeter}$ in Eqs. (5-6) derives the similar results, which are not shown in the paper. To compare the relative impact of different LULCC spatial downscaling methods (i.e. FLUS and Demeter) and future LULCC to carbon flux simulations, we further calculated the ratio (Φ_X) of the uncertainty from different LULCC spatial downscaling methods to the contribution of future LULCC to different carbon fluxes X as:

$$\Phi_X = \frac{RMSD^{X}_{FLUS,Demeter}}{RMSD^{X}_{FLUS,Reference}} \quad (7)$$

3 Results

3.1 Uncertain gridded LULCC projections

Results from the downscaling practices with Demeter and FLUS show large spatial difference between $LULCC_{FLUS}$ and $LULCC_{Demeter}$ under both SSP126 and SSP585. Figures S4 and S5 show the spatial patterns of future $LULCC_{Demeter}$ and $LULCC_{FLUS}$ in 2100 under SSP126 and SSP585, as well as the land cover map in 2015 as a reference. The FLUS and Demeter algorithms preserve the total area of each PFT, thus the Bias is relatively small. However, there is large difference in the spatial distributions of the four dominant PFTs over the ABoVE domain from 2020 to 2100, measured by RMSD (Figure 2). In general, the inconsistency between $LULCC_{Demeter}$ and $LULCC_{FLUS}$ rapidly increases in the first few decades and become stable afterwards under both SSP126 and SSP585, and the magnitudes and transition points are different across PFTs and scenarios (Figure 2) following the pattern of the input regional LULCC from GCAM (Figure S3).

The magnitudes are generally larger under SSP126 than those under SSP585 for all the dominant PFTs (Figures 2 and 3). For example, in 2100, the RMSDs between $LULCC_{Demeter}$ and $LULCC_{FLUS}$ are 15.9%, 11.5%, 18.1%, and 18.8%, respectively for the broadleaf deciduous boreal tree, needleleaf evergreen boreal tree, broadleaf deciduous boreal shrub, and C3 arctic grass under SSP126, while those values are 7.5%, 6.2%, 11. 6%, and 10.0%, respectively under SSP585.

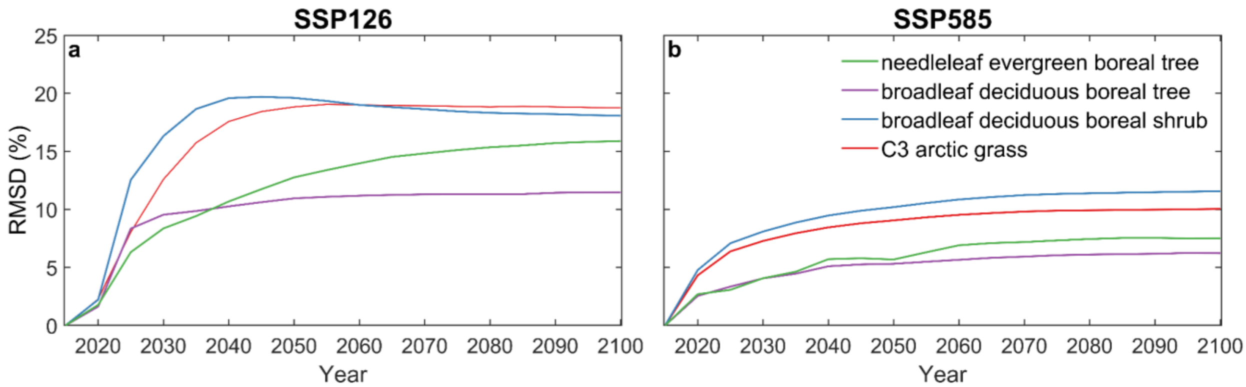

Figure 2. Time series of RMSD between $\mathrm{LULCC_{FLUS}}$ and $\mathrm{LULCC_{Demeter}}$ for 4 dominant CLM5_PFT types from 2020 to 2100 over the ABOVE domain under (a) SSP126 and (b) SSP585. Green, purple, blue, and red lines represent broadleaf deciduous boreal tree, needleleaf evergreen boreal tree, broadleaf deciduous boreal shrub, and C3 arctic grass separately. A larger RMSD value represents the larger difference between $\mathrm{LULCC_{FLUS}}$ and $\mathrm{LULCC_{Demeter}}$.

We further compared the areal fraction for four dominant PFTs from $\mathrm{LULCC_{Demeter}}$ and $\mathrm{LULCC_{FLUS}}$ in 2100 under both SSPs. As shown in Figure 3, the difference between $\mathrm{LULCC_{Demeter}}$ and $\mathrm{LULCC_{FLUS}}$ is not evenly distributed in the study domain under both SSPs. Under SSP126, compared to Demeter, FLUS prominently distributes up to 95% more needleleaf evergreen boreal trees and less boreal broadleaf deciduous trees in the northwestern ABoVE domain, and more boreal broadleaf deciduous shurbs and less C3 arctic grass in the northern area.

we observed similar spatial patterns in the differences between $\mathrm{LULCC_{FLUS}}$ and $\mathrm{LULCC_{Demeter}}$ under both SSPs, although with varying magnitudes. Positive values indicate that $\mathrm{LULCC_{FLUS}}$ has a greater proportion of the specific PFT compared to $\mathrm{LULCC_{Demeter}}$, while negative values indicate that $\mathrm{LULCC_{Demeter}}$ has a greater proportion of the PFT compared to $\mathrm{LULCC_{FLUS}}$. For needleleaf evergreen boreal trees, the major differences are found in the western region in Alaska. Under both SSPs, in the southeastern regions, the differences show opposite signs under the two SSPs, with negative values ($\mathrm{LULCC_{Demeter}}$ is larger) under SSP126 and positive values under SSP585. Southeastern regions show opposite signs of the differences between $\mathrm{LULCC_{FLUS}}$ and $\mathrm{LULCC_{Demeter}}$ under two scenarios with negative values under SSP126 but positive values under SSP585. For broadleaf deciduous boreal trees, under SSP126, $\mathrm{LULCC_{FLUS}}$ indicates more proportion in the southeastern ABoVE domain than $\mathrm{LULCC_{Demeter}}$, while under SSP585, $\mathrm{LULCC_{FLUS}}$ indicates smaller proportion in the northwestern regions, and up to 50% smaller proportion in the southeastern regions than $\mathrm{LULCC_{Demeter}}$. For broadleaf deciduous boreal shrub, $\mathrm{LULCC_{FLUS}}$ overall has a larger proportion in the northern regions than $\mathrm{LULCC_{Demeter}}$ under SSP126. Under SSP585, $\mathrm{LULCC_{FLUS}}$ shows a smaller proportion in the southwestern regions, and a larger value in the western and northern regions than $\mathrm{LULCC_{Demeter}}$. For C3 arctic grass, $\mathrm{LULCC_{FLUS}}$ shows larger differences from $\mathrm{LULCC_{Demeter}}$ with heterogenetic spatial distribution under SSP126, while their difference under SSP585 is smaller, but follows a similar spatial pattern with that under SSP126.

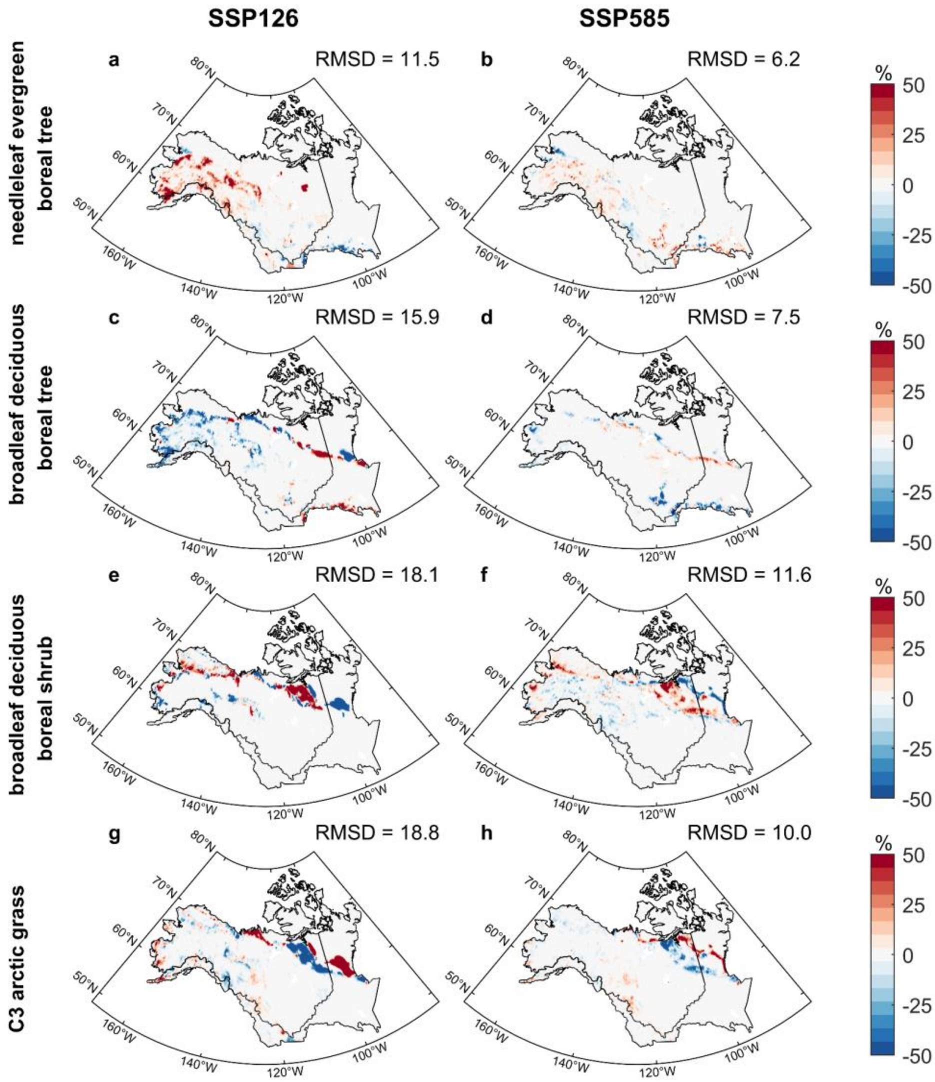

Figure 3. The spatial differences between $LULCC_{FLUS}$ and $LULCC_{Demeter}$ (calculated as $LULCC_{FLUS}$- $LULCC_{Demeter}$) in 2100 for the 4 dominant CLM5_PFT: (a-b) needleleaf evergreen boreal tree, (c-d) broadleaf deciduous boreal tree, (e-f) broadleaf deciduous boreal shrub, and (g-h) C3 arctic grass over the ABoVE domain under (a,c,e,g) SSP126 and (b,d,f,h) SSP585. The corresponding RMSD values (Unit: %) are shown in each panel. Positive values indicate larger PFT fraction by $LULCC_{FLUS}$.

3.2 Impacts of future LULCC uncertainty on terrestrial carbon cycle

Figure 4 shows the differences of CLM5 estimated annual carbon fluxes over the ABoVE domain from 2015 to 2100 between using $LULCC_{FLUS}$ and $LULCC_{Demeter}$ as well as those between using $LULCC_{FLUS}$ and $LULCC_{Reference}$. The RMSD between the results using $LULCC_{FLUS}$ and $LULCC_{Demeter}$ of the estimated carbon fluxes ($RMSD_{FLUS,Demeter}$) increases rapidly with time before 2040, and then becomes stable from 2040 to 2100 under both scenarios. The bias between the estimated carbon fluxes ($Bias_{FLUS,Demeter}$) decreases significantly before 2040 and fluctuates thereafter under SSP126, while such discrepancy is smaller and more stable under SSP585. Such temporal trends are similar to those the differences in the LULCC (Figure 2). By 2100, the $RMSD_{FLUS,Demeter}$ are 120.9, 107.4, and 53.3 gC m^{-2} year^{-1}for GPP, ER and NEE, respectively under SSP126, and are 53.3, 44.9, and 29.7 gC m^{-2} year^{-1}, respectively under SSP585 (Figure 4a,b; Table S1). The Biases in 2100 are -1.7, -1.9, and -0.1 gC m^{-2} year^{-1} under SSP126, and 4.6, -0.6, and -4.0 gC m^{-2} year^{-1} under SSP585 for GPP, ER and NEE, respectively (Figure 4c,d).

Besides, $RMSD_{FLUS,Demeter}$ is comparable to $RMSD_{FLUS,Reference}$. For example, in 2100, the ratios of the uncertainty from different LULCC spatial downscaling methods for GPP, ER, and NEE (Φ_{GPP}, Φ_{ER}, and Φ_{NEE}) are 79.6%, 83.7%, and 79.7%, respectively under SSP126, and are 98.4%, 93.7%, and 97.9% respectively under SSP585. Overall, the $Bias_{FLUS,Demeter}$ is smaller than $Bias_{FLUS,Reference}$ under SSP126, while under SSP585, the $Bias_{FLUS,Demeter}$ is similar to $Bias_{FLUS,Reference}$ and both of them are with small magnitudes.

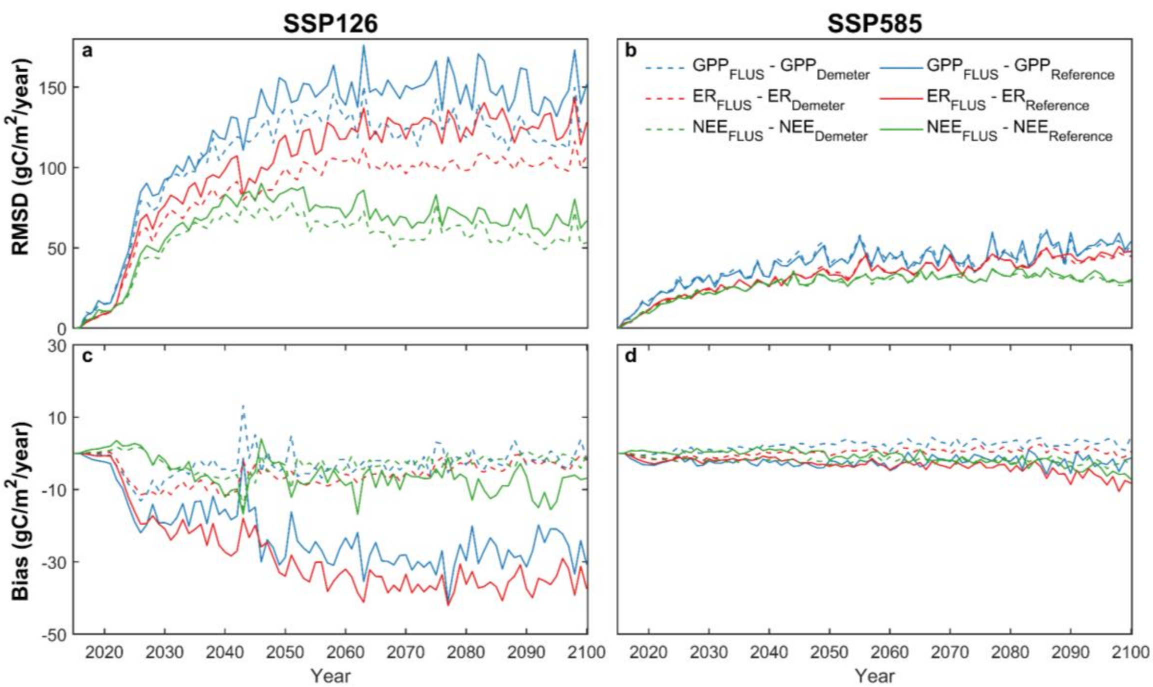

Figure 4. Time series of the RMSD and Bias in (blue) GPP, (red) ER, and (green) NEE, calculated based on the differences (dashed line) between the simulations using $LULCC_{FLUS}$ and $LULCC_{Demeter}$ and the difference (solid line) between the simulations using $LULCC_{FLUS}$ and historical LULCC in 2015, under (a, c) SSP126 and (b, d) SSP585.

We further compared the spatial pattern of the difference between GPP_{FLUS}, ER_{FLUS}, NEE_{FLUS} and $GPP_{Demeter}$, $ER_{Demeter}$, $NEE_{Demeter}$ under both scenarios (Figures 5, S6 and S7). Under SSP126, GPP_{FLUS} is larger in the northwestern regions, but is smaller in the eastern regions than $GPP_{Demeter}$ (Figure 5). The spatial pattern and magnitude of the difference in ER are similar as GPP. For NEE, the spatial pattern of the difference is similar to GPP and ER, but with smaller magnitude and opposite direction except for the southwestern regions. SSP585 shows smaller differences in GPP, ER, and NEE than SSP126 (Figure 5). Under SSP585, the spatial pattern, signs, and magnitudes of the differences in GPP and ER are similar. Positive values can be observed in the southern, central, and western regions, while negative values are present in the southeastern and eastern regions. For NEE, NEE_{FLUS} shows smaller values in the southwestern but larger values in the northwestern and eastern regions than $NEE_{Demeter}$. To better attribute the difference between GPP_{FLUS}, ER_{FLUS}, NEE_{FLUS} and $GPP_{Demeter}$, $ER_{Demeter}$, $NEE_{Demeter}$ to the uncertainty in gridded LULCC projections, we further investigated the relationship between the difference between $LULCC_{FLUS}$ and $LULCC_{Demeter}$ for each PFT and the difference in GPP, ER, and NEE estimations (Figures 6 and S8). Overall, we found that the grid cells with larger difference between $LULCC_{FLUS}$ and $LULCC_{Demeter}$ correspond to larger differences in all the GPP, ER, and NEE under both SSP126 and SSP585.

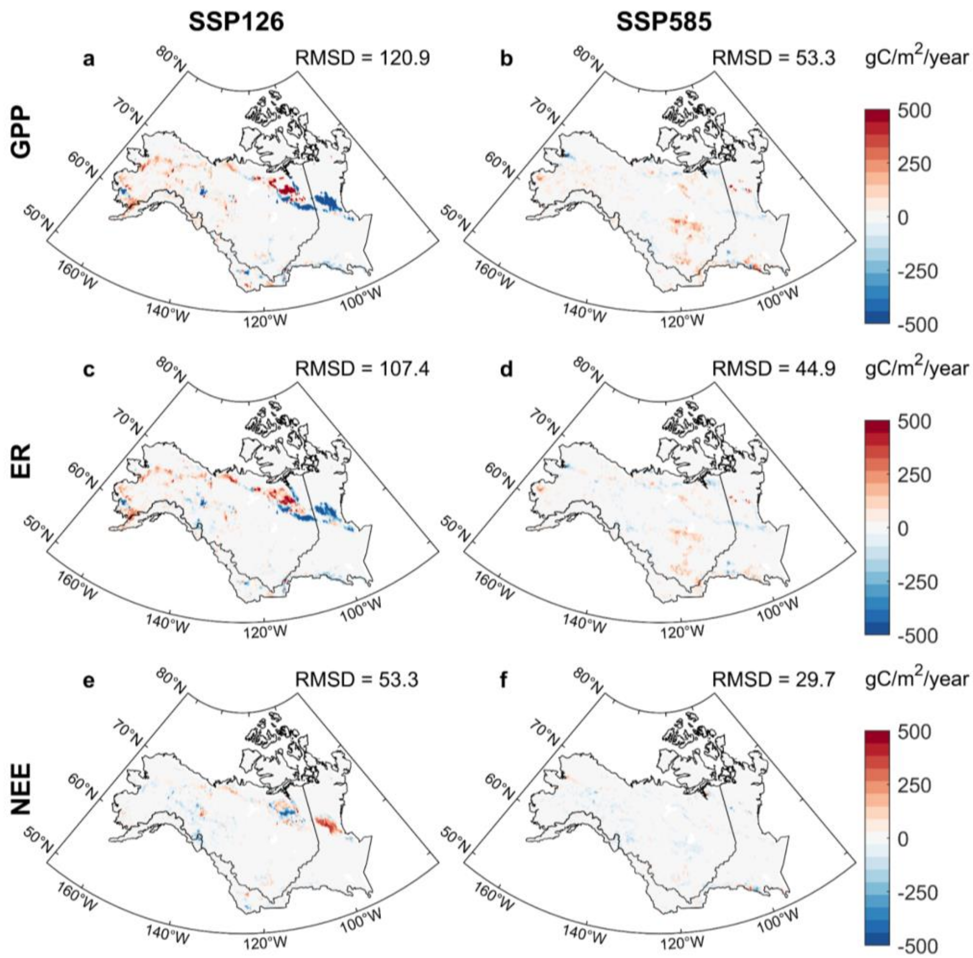

Figure 5. The spatial pattern for the differences of (a-b) GPP_{FLUS} vs $GPP_{Demeter}$, (c-d) ER_{FLUS} vs $ER_{Demeter}$, and (e-f) NEE_{FLUS} vs $NEE_{Demeter}$ in 2100 between CLM5 simulations under (a,c,e) SSP126 and (b,d,f) SSP585. The corresponding $RMSD_{FLUS,Demeter}$ values are shown in each panel.

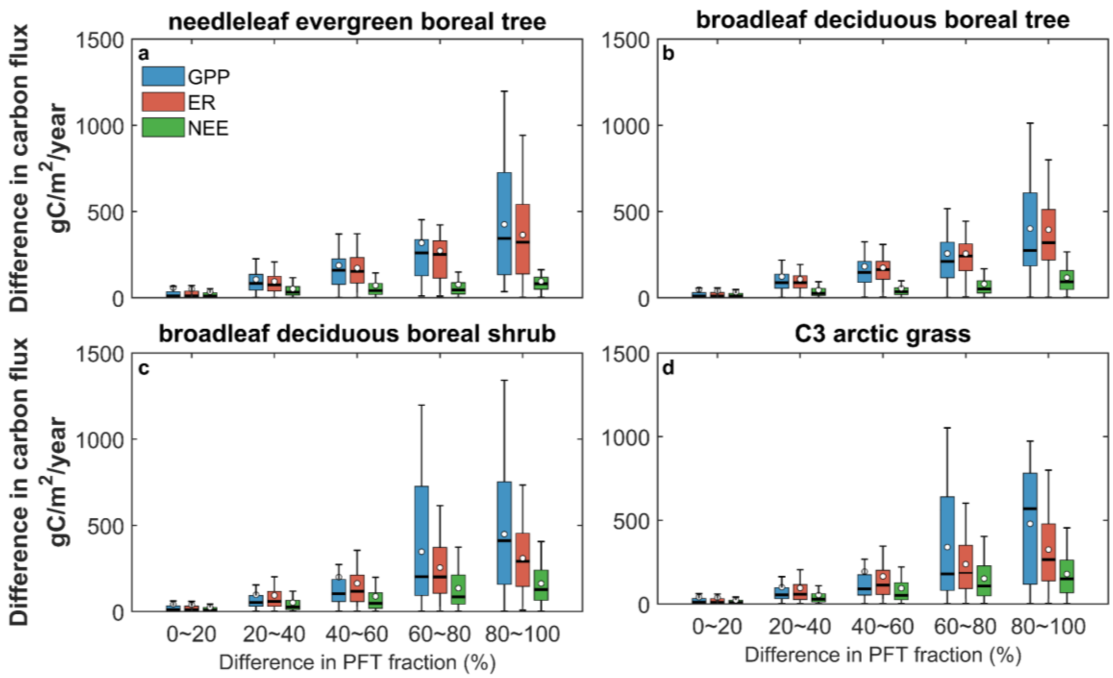

Figure 6. The relationship of the absolute difference in PFT fraction between $LULCC_{FLUS}$ and $LULCC_{Demeter}$ with the corresponding absolute difference in GPP (blue), ER (red), and NEE (green) under SSP126 for 4 PFTs: (a) needleleaf evergreen boreal tree, (b) broadleaf deciduous boreal tree, (c) broadleaf deciduous boreal shrub, and (d) C3 arctic grass.

4 Discussion

Previous studies show that LULCC can cause large uncertainties of carbon cycle estimates that is equivalent to 80% of the net effects of CO_2 and climate(Di Vittorio et al., 2018). There are diverse factors that could contribute to the uncertainties of future gridded LULCC projections. In this study, we focused on quantifying the uncertainty induced by different spatial downscaling methods. Our results indicate that the differences arising from different spatial downscaling methods can be as large as 19% in terms of the RMSD for a single CLM5_PFT type in 2100 in our study region. Furthermore, the impacts of spatial downscaling methods vary with scenarios. The difference between $LULCC_{Demeter}$ and $LULCC_{FLUS}$ increases more rapidly in the first few decades under SSP126 than SSP585 (Figure 2), due to the more rapid increase of regional LULCC projections from GCAM under SSP126. The overall lower $RMSD_{FLUS,Demeter}$ values under SSP585 than under SSP126 is possibly due to the smaller projected regional LULCC from GCAM under SSP585 compared to SSP126 (Figure S5).

Although we observed large spatial discrepancies in projected carbon fluxes due to LULCC differences resulting from different spatial downscaling methods, the discrepancies in projected regional average carbon fluxes are relatively small (Figure 4). Our results are consistent with previous observational-based studies (Dashti et al., 2022), which attributed this phenomenon to the cancellation of opposing signs within a small region with similar climate forcings. Furthermore, the uncertainty of the estimated carbon fluxes from the spatial downscaling methods is generally lower under SSP585 compared to that under SSP126, due to smaller differences between

$LULCC_{Demeter}$ and $LULCC_{FLUS}$ under SSP585 than SSP126. Overall, the impacts of uncertain LULCC on carbon fluxes because of the spatial downscaling process are comparable to the impacts due to future LULCC itself (Figure 4). These stress the importance of considering the uncertainties of the LULCC spatial downscaling methods in carbon cycle projections.

It is important to note that existing spatial downscaling algorithms are inherently different, despite being developed with the same objective. For example, there are several notable differences between Demeter and FLUS that may contribute to the discrepancies between the resulted LULCC product. First, Demeter and FLUS employ different algorithms/methods to determine land types and their respective area proportions in a given grid cell (Li et al., 2017; Liu et al., 2017). Theoretically, Demeter only captures the net change of LULCC (Page et al., 2016; West et al., 2014), while FLUS simulates both gross and net LULCC change. For example, with a given decreased area of shrub from GCAM, we found that Demeter only simulated the shrinkage in shrub under SSP126, while FLUS simulates the shrinkage in most regions and expansions in some parts of the ABoVE domain, reflecting the different assumptions of the two models. Specifically, Demeter assumes that an increasing land type can only encroach a decreasing land type, and a decreasing land type can only be encroached by an increasing land type. These results in that a decreasing land type can only shrink and an increasing land type can only expand or intensify. In contrast, FLUS estimates the combined probabilities for each land type in each grid cell (Li et al., 2017; Liu et al., 2017). making it possible for a decreasing land type to expand in some regions and vice versa. Second, the spatial factors that regulate the downscaling processes in Demeter and FLUS are also different. Demeter has a set of default spatial factors that focus on soil conditions such as soil workability and nutrient availability. In contrast, FLUS typically include the soil condition along with many other spatial factors including climate background (i.e., precipitation and temperature), environmental conditions (e.g., elevation), and socioeconomic factors (i.e., city centers and transportation). In this study, we aim to represent the general performance of both spatial downscaling methods. Thus, we used the default soil conditions for Demeter, and commonly used multiple spatial factors listed in Table 2 for FLUS. Using different spatial factors may also cause the difference in the spatial pattern of the final downscaled LULCC, since these factors are important for estimating the occurrence probability of each land type at a specific grid cell, referred to as probability-of-occurrence in FLUS and suitability index in Demeter (Chen et al., 2019).

Careful consideration of data characteristics, research goals, and future scenarios are critical when selecting a LULCC spatial downscaling method. Additionally, it is important to evaluate the performance and uncertainty of different methods. We recommend selecting the more suitable LULCC spatial downscaling methods based on the research requirements and the unique characteristics of each method. For example, when the land type in the regional projections is different from the land type in the base map, Demeter can be more convenient than FLUS because Demeter can avoid the post-processing steps, e.g., LULCC reclassification. If the study focuses more on the gross LULCC change rather than only the net change, FLUS may be a better choice. Compared to FLUS, Demeter does not consider socioeconomic and environment factors other than soil condition by default, but user can add those factors into Demeter based on their need. It is important to point out there are more spatial downscaling methods beyond the two models discussed in this study, such as Global Land-use Model 2, and Platform for Land-Use and Environmental Model, and thus the uncertainty analyzed here could be possibly even larger than what we show here. Thus, we appeal for attention on the uncertainties of gridded future LULCC data and their applications caused by different spatial downscaling methods, which could be taken into consideration in the future phases of climate model intercomparison project. This study is limited in the ABoVE region, and future studies could expand the scope to other regions and the globe.

5 Conclusions

In this study, we investigated the impact of using different spatial downscaling methods on LULCC projections and their associated impacts on ecosystem carbon fluxes under two global change scenarios. We compared the results from two popular spatial downscaling methods, Demeter and FLUS, using the same regional area projections. Our findings showed that different spatial downscaling methods can result in large differences in the spatial pattern of LULCC and can further induce substantial variations in carbon cycle simulations. Importantly, the uncertainty introduced by spatial downscaling methods is comparable to the uncertainty arising from future LULCC on carbon cycle projections. Additionally, we observed that the uncertainties introduced by spatial downscaling methods under SSP126 were generally larger than those under SSP585, for both gridded LULCC and carbon cycle dynamics. This study highlights the importance of carefully considering the uncertainties associated with spatial downscaling processes and their implications for downstream applications. To address these uncertainties, we recommend choosing the most appropriate spatial downscaling method based on research requirements and unique characteristics of each method.

Acknowledgments

This research was supported by the National Aeronautics and Space Administration (NASA) through Terrestrial Ecology: Arctic Boreal Vulnerability Experiment (ABoVE) grants NNH18ZDA001N (award number 80HQTR19T0055) to Min Chen.

Open Research

MODIS LULCC data are publicly accessible at the Google Earth Engine Platform: https://developers.google.com/earth-engine/datasets/catalog/MODIS_061_MCD12Q1. The future LULCC and carbon flux data is available at https://doi.org/10.6084/m9.figshare.22236652.v4.
The GCAM model can be freely downloaded in https://github.com/JGCRI/gcam-core/releases.
Demeter and FLUS are freely available from https://github.com/JGCRI/demeter, and http://www.geosimulation.cn/FLUS.html, respectively.

References

Alcaraz-Segura, D., Chuvieco, E., Epstein, H. E., Kasischke, E. S., & Trishchenko, A. (2010). Debating the greening vs. browning of the North American boreal forest: Differences between satellite datasets. *Global Change Biology*, *16*(2), 760–770. https://doi.org/10.1111/j.1365-2486.2009.01956.x

Alexander, P., Prestele, R., Verburg, P. H., Arneth, A., Baranzelli, C., Batista e Silva, F., Brown, C., Butler, A., Calvin, K., Dendoncker, N., Doelman, J. C., Dunford, R., Engström, K., Eitelberg, D., Fujimori, S., Harrison, P. A., Hasegawa, T., Havlik, P., Holzhauer, S., … Rounsevell, M. D. A. (2017). Assessing uncertainties in land cover projections. *Global Change Biology*, *23*(2), 767–781. https://doi.org/10.1111/gcb.13447

Bonan, G. B., & Doney, S. C. (2018). Climate, ecosystems, and planetary futures: The challenge to predict life in Earth system models. *Science*, *359*(6375). https://doi.org/10.1126/science.aam8328

Bonan, G. B., Levis, S., Kergoat, L., & Oleson, K. W. (2002). Landscapes as patches of plant functional types: An integrating concept for climate and ecosystem models. *Global Biogeochemical Cycles*, *16*(2), 5-1-5–23. https://doi.org/10.1029/2000gb001360

Bukovsky, M. S., Gao, J., Mearns, L. O., & O'Neill, B. C. (2021). SSP-Based Land-Use Change Scenarios: A Critical Uncertainty in Future Regional Climate Change Projections. *Earth's Future*, *9*(3), 1–18. https://doi.org/10.1029/2020EF001782

Cao, M., Zhu, Y., Quan, J., Zhou, S., Lü, G., & Chen, M. (2010). *Spatial sequential modeling and predication of global land use and land cover changes by integrating a global change assessment model and cellular automata*. 0–1. https://doi.org/10.1029/2019EF001228

Chen, C., Park, T., Wang, X., Piao, S., Xu, B., Chaturvedi, R. K., Fuchs, R., Brovkin, V., Ciais, P., Fensholt, R., Tømmervik, H., Bala, G., Zhu, Z., Nemani, R. R., & Myneni, R. B. (2019). China and India lead in greening of the world through land-use management. *Nature Sustainability*, *2*(2), 122–129. https://doi.org/10.1038/s41893-019-0220-7

Chen, G., Li, X., Liu, X., Chen, Y., Liang, X., Leng, J., Xu, X., Liao, W., Qiu, Y., Wu, Q., & Huang, K. (2020a). Global projections of future urban land expansion under shared socioeconomic pathways. *Nature Communications*, *11*(1), 1–12. https://doi.org/10.1038/s41467-020-14386-x

Chen, M., Vernon, C. R., Graham, N. T., Hejazi, M., Huang, M., Cheng, Y., & Calvin, K. (2020b). Global land use projections for 2015-2100 at 0.05-degree resolution under diverse Shared Socioeconomic Pathways and Representative Concentration Pathways. *Scientific Data*, Submitted. https://doi.org/10.1038/s41597-020-00669-x

Chen, M., Vernon, C. R., Huang, M., Calvin, K. v, Kraucunas, I. P., Northwest, P., Division, G. C., & Northwest, P. (2019). *Calibration and analysis of the uncertainty in downscaling global land use and land cover projections from GCAM using Demeter (v1.0.0)*. 1753–1764.

Cheng, Y., Huang, M., Zhu, B., Bisht, G., Zhou, T., Liu, Y., Song, F., & He, X. (2021). Validation of the Community Land Model Version 5 Over the Contiguous United States (CONUS) Using In Situ and Remote Sensing Data Sets. *Journal of Geophysical Research: Atmospheres*, *126*(5), 1–27. https://doi.org/10.1029/2020JD033539

Dashti, H. *et al.* Underestimation of the impact of land cover change on the biophysical environment of the Arctic and Boreal Region of North America. *Environmental Research Letters* (2022) doi:10.1088/1748-9326/ac8da7.

Di Vittorio, A. V., Mao, J., Shi, X., Chini, L., Hurtt, G., & Collins, W. D. (2018). Quantifying the Effects of Historical Land Cover Conversion Uncertainty on Global Carbon and Climate Estimates. *Geophysical Research Letters*, *45*(2), 974–982. https://doi.org/10.1002/2017GL075124

Doelman, J. C., Stehfest, E., Tabeau, A., van Meijl, H., Lassaletta, L., Gernaat, D. E. H. J., Neumann-Hermans, K., Harmsen, M., Daioglou, V., Biemans, H., van der Sluis, S., & van Vuuren, D. P. (2018). Exploring SSP land-use dynamics using the IMAGE model: Regional and gridded scenarios of land-use change and land-based climate change mitigation. *Global Environmental Change*, *48*(December 2017), 119–135. https://doi.org/10.1016/j.gloenvcha.2017.11.014

Dong, N., You, L., Cai, W., Li, G., & Lin, H. (2018). Land use projections in China under global socioeconomic and emission scenarios: Utilizing a scenario-based land-use change assessment framework. *Global Environmental Change*, *50*(April), 164–177. https://doi.org/10.1016/j.gloenvcha.2018.04.001

Duveiller, G., Hooker, J., & Cescatti, A. (2018). The mark of vegetation change on Earth's surface energy balance. *Nature Communications*, *9*(1). https://doi.org/10.1038/s41467-017-02810-8

Fick, S. E., & Hijmans, R. J. (2017). WorldClim 2: new 1-km spatial resolution climate surfaces for global land areas. *International Journal of Climatology*, *37*(12), 4302–4315. https://doi.org/10.1002/joc.5086

Findell, K. L., Berg, A., Gentine, P., Krasting, J. P., Lintner, B. R., Malyshev, S., Santanello, J. A., & Shevliakova, E. (2017). The impact of anthropogenic land use and land cover change on regional climate extremes. *Nature Communications*, *8*(1), 1–9. https://doi.org/10.1038/s41467-017-01038-w

Friedl, M. A., Sulla-Menashe, D., Tan, B., Schneider, A., Ramankutty, N., Sibley, A., & Huang, X. (2010). MODIS Collection 5 global land cover: Algorithm refinements and characterization of new datasets. *Remote Sensing of Environment*, *114*(1), 168–182. https://doi.org/10.1016/j.rse.2009.08.016

Friedlingstein, P., Jones, M., Sullivan, M. O., & Hauck, J. (2021). *Global Carbon Budget 2021*. *November*. https://doi.org/10.5194/essd-2021-386

Fujimori, S., Hasegawa, T., Ito, A., Takahashi, K., & Masui, T. (2018). Data descriptor: Gridded emissions and land-use data for 2005–2100 under diverse socioeconomic and climate mitigation scenarios. *Scientific Data*, *5*, 1–13. https://doi.org/10.1038/sdata.2018.210

Fujimori, S., Masui, T., & Matsuoka, Y. (2014). Development of a global computable general equilibrium model coupled with detailed energy end-use technology. *Applied Energy*, *128*, 296–306. https://doi.org/10.1016/j.apenergy.2014.04.074

Guivarch, C., Le Gallic, T., Bauer, N., Fragkos, P., Huppmann, D., Jaxa-Rozen, M., Keppo, I., Kriegler, E., Krisztin, T., Marangoni, G., Pye, S., Riahi, K., Schaeffer, R., Tavoni, M., Trutnevyte, E., van Vuuren, D., & Wagner, F. (2022). Using large ensembles of climate change mitigation scenarios for robust insights. *Nature Climate Change*, *12*(5), 428–435. https://doi.org/10.1038/s41558-022-01349-x

Harris, N. L., Gibbs, D. A., Baccini, A., Birdsey, R. A., de Bruin, S., Farina, M., Fatoyinbo, L., Hansen, M. C., Herold, M., Houghton, R. A., Potapov, P. v., Suarez, D. R., Roman-Cuesta, R. M., Saatchi, S. S., Slay, C. M., Turubanova, S. A., & Tyukavina, A. (2021). Global maps of twenty-first century forest carbon fluxes. *Nature Climate Change*, *11*(3), 234–240. https://doi.org/10.1038/s41558-020-00976-6

Hengl, T. (2018). *Global DEM derivatives at 250 m, 1 km and 2 km based on the MERIT DEM [Dataset]*. Zenodo. https://doi.org/https://doi.org/10.5281/zenodo.1447210

Huang, Z., Wu, X., Garcia, A. J., Fik, T. J., & Tatem, A. J. (2013). *An Open-Access Modeled Passenger Flow Matrix for the Global Air Network in 2010*. *8*(5). https://doi.org/10.1371/journal.pone.0064317

Hurtt, G., Chini, L., Sahajpal, R., Frolking, S., Bodirsky, B., Calvin, K., Doelman, J., Fisk, J., Fujimori, S., Goldewijk, K. K., Hasegawa, T., Havlik, P., Heinimann, A., Humpenöder, F., Jungclaus, J., Kaplan, J., Kennedy, J., Kristzin, T., Lawrence, D., … Zhang, X. (2020). Harmonization of Global Land-Use Change and Management for the Period 850–2100 (LUH2) for CMIP6. *Geoscientific Model Development Discussions*, *April*, 1–65. https://doi.org/10.5194/gmd-2019-360

Calvin, K., Bond-Lamberty, B., Clarke, L., Edmonds, J., Eom, J., Hartin, C., Kim, S., Kyle, P., Link, R., Moss, R., McJeon, H., Patel, P., Smith, S., Waldhoff, S., & Wise, M. (2017). The SSP4: A world of deepening inequality. *Global Environmental Change*, *42*, 284–296. https://doi.org/10.1016/j.gloenvcha.2016.06.010

Calvin, K., Patel, P., Clarke, L., Asrar, G., Bond-lamberty, B., Cui, R. Y., Vittorio, A. di, Dorheim, K., Edmonds, J., Hartin, C., Hejazi, M., Horowitz, R., Iyer, G., Kyle, P., Kim, S., Link, R., Mcjeon, H., Smith, S. J., Snyder, A., … Calvin, C. K. (2019). *GCAM v5 . 1 : representing the linkages between energy , water , land , climate , and economic systems*. 677–698.

Lawrence, D. M., Fisher, R. A., Koven, C. D., Oleson, K. W., Swenson, S. C., Bonan, G., Collier, N., Ghimire, B., van Kampenhout, L., Kennedy, D., Kluzek, E., Lawrence, P. J., Li, F., Li, H., Lombardozzi, D., Riley, W. J., Sacks, W. J., Shi, M., Vertenstein, M., … Zeng, X. (2019). The Community Land Model Version 5: Description of New Features, Benchmarking, and Impact of Forcing Uncertainty. *Journal of Advances in Modeling Earth Systems*, *11*(12), 4245–4287. https://doi.org/10.1029/2018MS001583

Li, X., Chen, G., Liu, X., Liang, X., Wang, S., Chen, Y., Pei, F., & Xu, X. (2017). A New Global Land-Use and Land-Cover Change Product at a 1-km Resolution for 2010 to 2100 Based on Human–Environment Interactions. *Annals of the American Association of Geographers*, *107*(5), 1040–1059. https://doi.org/10.1080/24694452.2017.1303357

Liao, W., Liu, X., Xu, X., Chen, G., Liang, X., Zhang, H., & Li, X. (2020). Projections of land use changes under the plant functional type classification in different SSP-RCP scenarios in China. *Science Bulletin*, *xxxx*. https://doi.org/10.1016/j.scib.2020.07.014

Liu, J., Wennberg, P. O., Parazoo, N. C., Yin, Y., & Frankenberg, C. (2020). Observational Constraints on the Response of High-Latitude Northern Forests to Warming. *AGU Advances*, *1*(4). https://doi.org/10.1029/2020av000228

Liu, X., Liang, X., Li, X., Xu, X., Ou, J., Chen, Y., Li, S., Wang, S., & Pei, F. (2017a). A future land use simulation model (FLUS) for simulating multiple land use scenarios by coupling human and natural effects. *Landscape and Urban Planning*, *168*(November), 94–116. https://doi.org/10.1016/j.landurbplan.2017.09.019

Luo, M., Hu, G., Chen, G., Liu, X., Hou, H., & Li, X. (2022). 1 km land use/land cover change of China under comprehensive socioeconomic and climate scenarios for 2020–2100. *Scientific Data*, *9*(1), 1–13. https://doi.org/10.1038/s41597-022-01204-w

Ma, L., Hurtt, G., Chini, L., Sahajpal, R., Pongratz, J., Frolking, S., Stehfest, E., Klein Goldewijk, K., O' Leary, D., & Doelman, J. (2019). Global Transition Rules for Translating Land-use Change (LUH2) To Land-cover Change for CMIP6 using GLM2. *Geoscientific Model Development*, *July*, 1–30. https://doi.org/10.5194/gmd-2019-146-supplement

Mekonnen, Z. A., Riley, W. J., Berner, L. T., Bouskill, N. J., Torn, M. S., Iwahana, G., Breen, A. L., Myers-Smith, I. H., Criado, M. G., Liu, Y., Euskirchen, E. S., Goetz, S. J., Mack, M. C., & Grant, R. F. (2021). Arctic tundra shrubification: a review of mechanisms and impacts on ecosystem carbon balance. In *Environmental Research Letters* (Vol. 16, Issue 5). IOP Publishing Ltd. https://doi.org/10.1088/1748-9326/abf28b

Page, Y. Le, West, T. O., Link, R., & Patel, P. (2016). *Downscaling land use and land cover from the Global Change Assessment Model for coupling with Earth system models*. 3055–3069. https://doi.org/10.5194/gmd-9-3055-2016

Pastick, N. J., Jorgenson, M. T., Goetz, S. J., Jones, B. M., Wylie, B. K., Minsley, B. J., Genet, H., Knight, J. F., Swanson, D. K., & Jorgenson, J. C. (2019). Spatiotemporal remote sensing of ecosystem change and causation across Alaska. *Global Change Biology*, *25*(3), 1171–1189. https://doi.org/10.1111/gcb.14279

Popp, A., Humpenöder, F., Weindl, I., Bodirsky, B. L., Bonsch, M., Lotze-Campen, H., Müller, C., Biewald, A., Rolinski, S., Stevanovic, M., & Dietrich, J. P. (2014). Land-use protection for climate change mitigation. *Nature Climate Change*, *4*(12), 1095–1098. https://doi.org/10.1038/nclimate2444

Riahi, K., Vuuren, D. P. Van, Kriegler, E., Edmonds, J., Neill, B. C. O., Fujimori, S., Bauer, N., Calvin, K., Dellink, R., Fricko, O., Lutz, W., Popp, A., Crespo, J., Kc, S., Leimbach, M., Jiang, L., Kram, T., Rao, S., Emmerling, J., … Tavoni, M. (2017). *The Shared Socioeconomic Pathways and their energy , land use , and greenhouse gas emissions implications : An overview*. *42*, 153–168. https://doi.org/10.1016/j.gloenvcha.2016.05.009

Semenchuk, P., Plutzar, C., Kastner, T., Matej, S., Bidoglio, G., Erb, K. H., Essl, F., Haberl, H., Wessely, J., Krausmann, F., & Dullinger, S. (2022). Relative effects of land conversion and land-use intensity on terrestrial vertebrate diversity. *Nature Communications*, *13*(1). https://doi.org/10.1038/s41467-022-28245-4

Song, X. P., Hansen, M. C., Stehman, S. V., Potapov, P. V., Tyukavina, A., Vermote, E. F., & Townshend, J. R. (2018). Global land change from 1982 to 2016. *Nature*, *560*(7720), 639–643. https://doi.org/10.1038/s41586-018-0411-9

Sterling, S. M., Ducharne, A., & Polcher, J. (2013). The impact of global land-cover change on the terrestrial water cycle. *Nature Climate Change*, *3*(4), 385–390. https://doi.org/10.1038/nclimate1690

Vernon, C. R., Page, Y. Le, Chen, M., Huang, M., Calvin, K. V, Kraucunas, P., & Braun, C. J. (2018). Demeter – A Land Use and Land Cover Change Disaggregation Model. *Journal of Open Research Software*, *6*(1), 15. https://doi.org/http://doi.org/10.5334/jors.208

West, T. O., Brandt, C. C., Baskaran, L. M., Hellwinckel, C. M., Mueller, R., Bernacchi, C. J., Bandaru, V., Yang, B., Wilson, B. S., Marland, G., Nelson, R. G., De La Torre Ugarte, D. G., & Post, W. M. (2010). Cropland carbon fluxes in the United States: Increasing geospatial resolution of inventory-based carbon accounting. *Ecological Applications*, *20*(4), 1074–1086. https://doi.org/10.1890/08-2352.1

West, T. O., Page, Y. Le, Huang, M., Wolf, J., & Thomson, A. M. (2014). *Downscaling global land cover projections from an integrated assessment model for use in regional analyses : results and evaluation for the US from 2005 to 2095*. https://doi.org/10.1088/1748-9326/9/6/064004

Wu, W., Hasegawa, T., Ohashi, H., Hanasaki, N., Liu, J., Matsui, T., Fujimori, S., Masui, T., & Takahashi, K. (2019). Global advanced bioenergy potential under environmental protection policies and societal transformation measures. *GCB Bioenergy*, *11*(9), 1041–1055. https://doi.org/10.1111/gcbb.12614

[Earth's Future]

Supporting Information for

Uncertain spatial pattern of future land use and land cover change and its impacts on terrestrial carbon cycle over the Arctic–Boreal region of North America

Meng Luo[1], Fa Li[1], Dalei Hao[2], Qing Zhu[3], Hamid Dashti[1], Min Chen[1]

[1]Department of Forest and Wildlife Ecology, University of Wisconsin-Madison, Madison, WI, USA.

[2]Atmospheric Sciences and Global Change Division, Pacific Northwest National Laboratory, Richland, WA, USA

[3]Climate and Ecosystem Sciences Division, Lawrence Berkeley National Laboratory, Berkeley, CA, USA.

Corresponding author: Min Chen (mchen392@wisc.edu)

Contents of this file

Figures S1 to S8
Tables S1

Introduction

The supplementary materials include 2 flowcharts that illustrate the procedure of future gridded LULCC projections using FLUS and Demeter and subsequent carbon cycle simulations, and 6 figures and 1 table that show the spatio-temporal comparison between LULCC downscaled by FLUS and Demeter, and carbon flux projections using the two downscaled LULCC data.

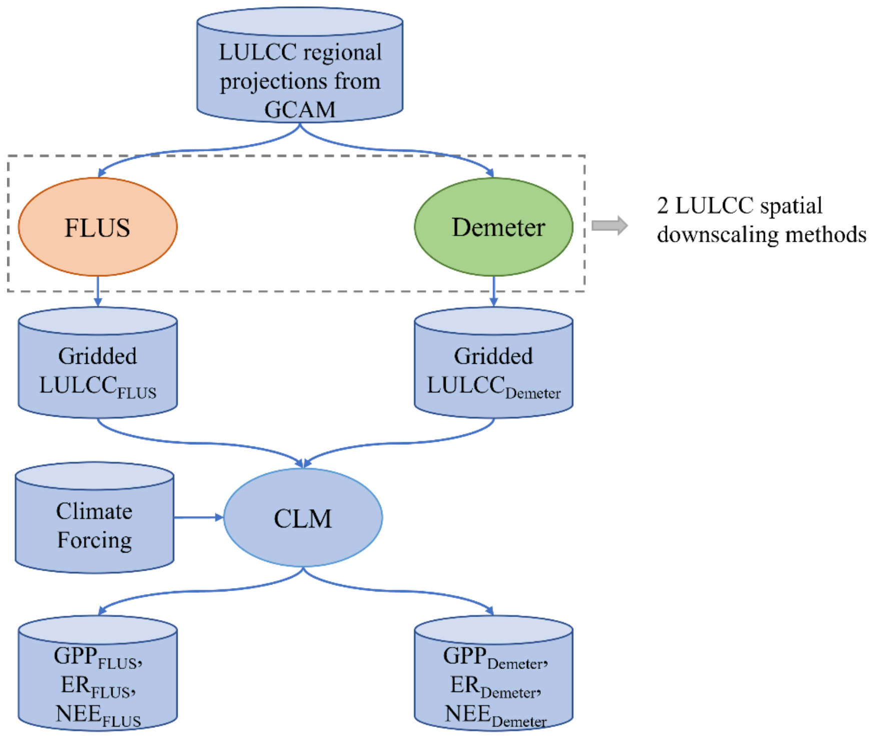

Figure S1. Flowchart of future gridded LULCC projections using FLUS and Demeter and subsequent carbon cycle simulations.

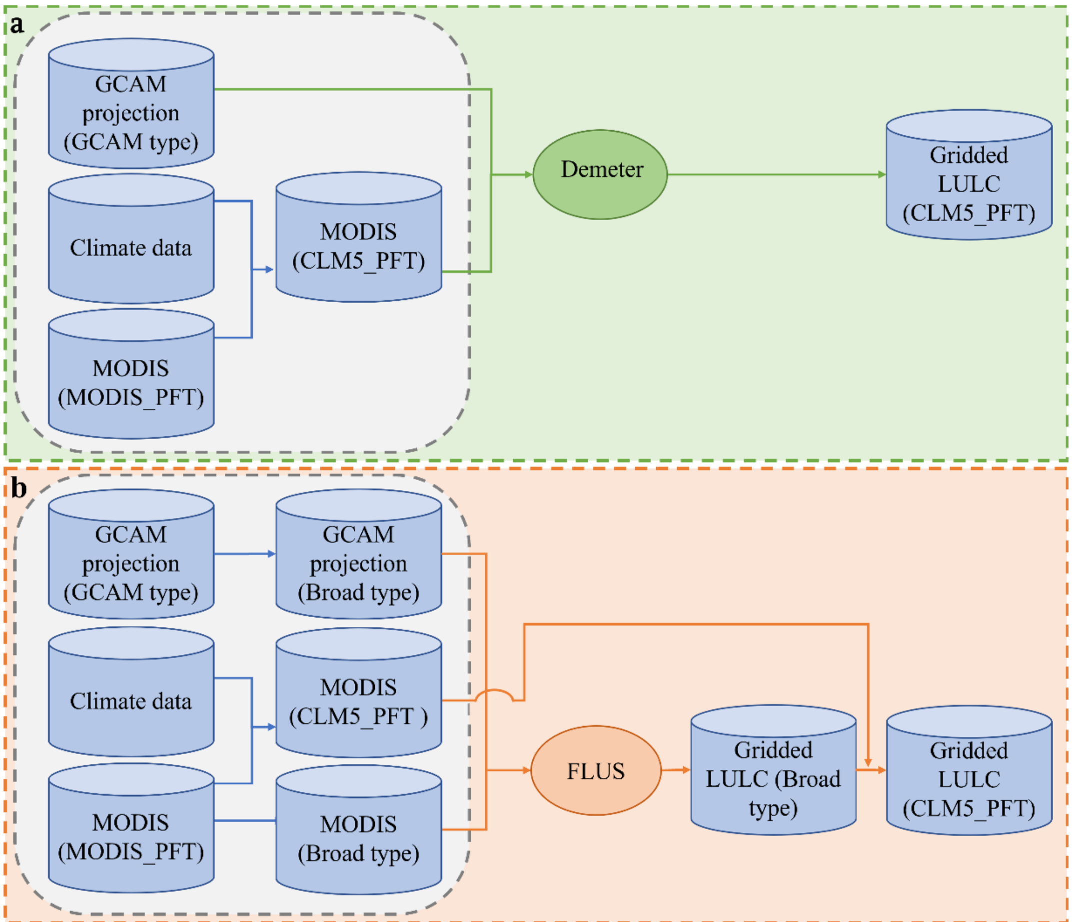

Figure S2. Schemes of LULCC reclassification and harmonization during the spatial downscaling process using Demeter and FLUS.

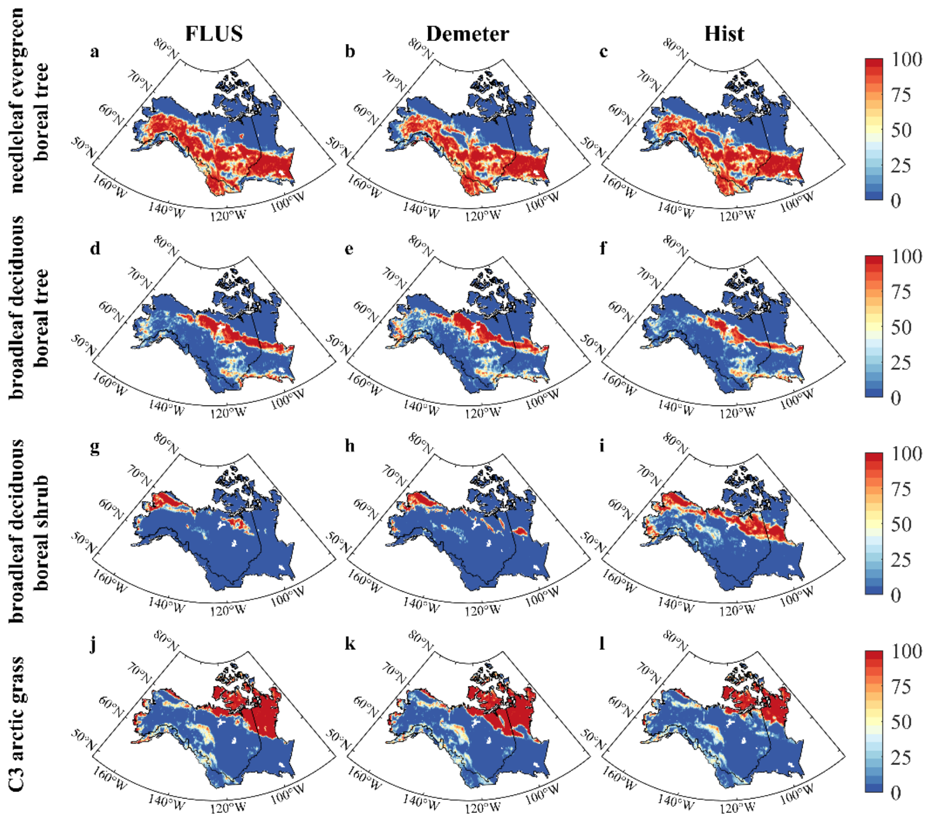

Figure S3. The spatial pattern of $LULCC_{FLUS}$ (a, d, g, j) and $LULCC_{Demeter}$ (b, e, h, l) in 2100 for SSP126 and historical LULCC in 2015 (c, f, i, l) over the ABoVE domain for the 4 dominant CLM5_PFT: (a-c) needleleaf evergreen boreal tree, (d-f) broadleaf deciduous boreal tree, (g-i) broadleaf deciduous boreal shrub, and (j-l) C3 arctic grass. The color with blue (red) represents there is small (large) area fraction of a specific CLM5_PFT.

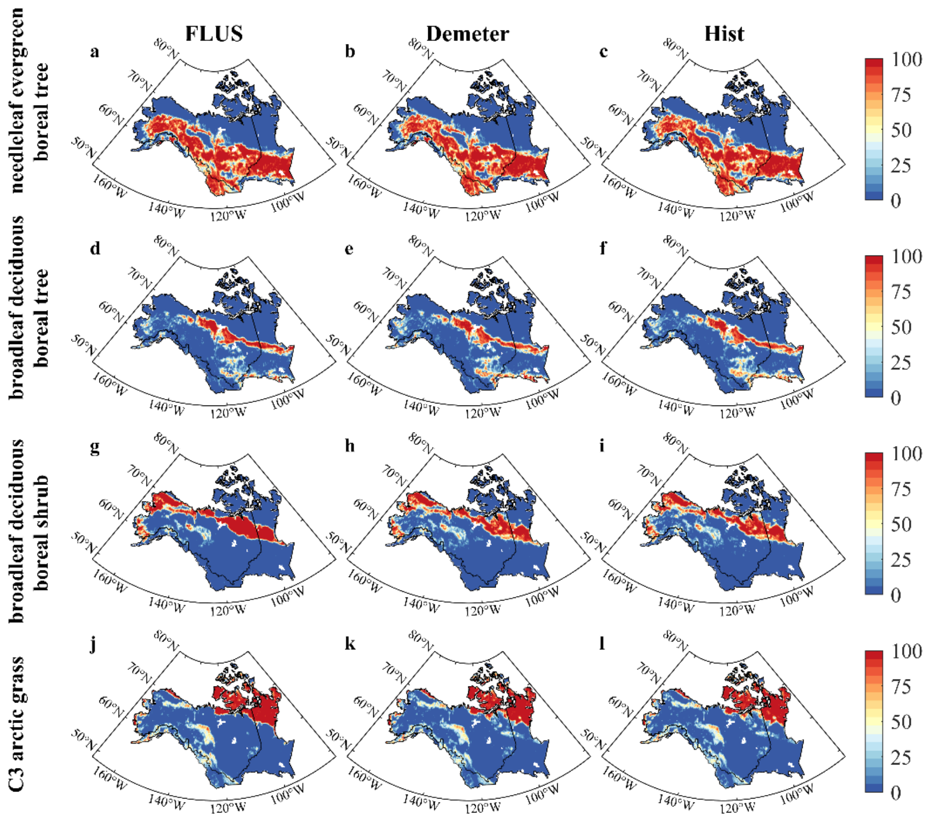

Figure S4. The spatial pattern of $LULCC_{FLUS}$ (a, d, g, j) and $LULCC_{Demeter}$ (b, e, h, k) in 2100 for SSP585 and historical LULCC in 2015 (c, f, i, l) over the ABoVE domain for the 4 dominant CLM5_PFT: (a-c) needleleaf evergreen boreal tree, (d-f) broadleaf deciduous boreal tree, (g-i) broadleaf deciduous boreal shrub, and (j-l) C3 arctic grass. The color with blue (red) represents there is small (large) area fraction of a specific CLM5_PFT.

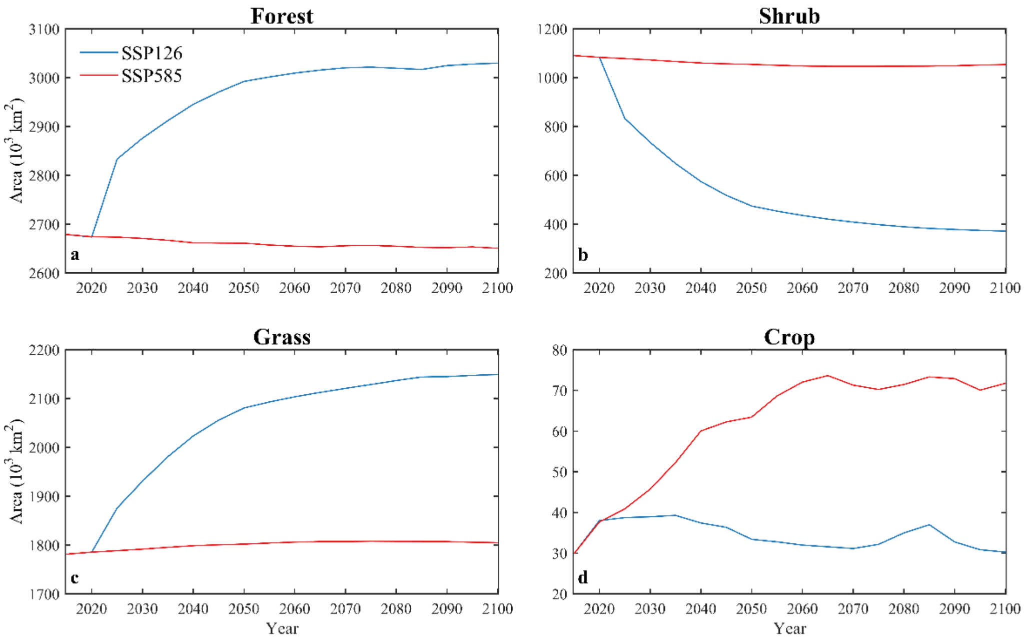

Figure S5. Time series of the harmonized LULCC area projections of four dominant broad LULCC types: (a) Forest, (b) Shrub, (c) Grass, (d) Crop from GCAM during 2015-2100 over the main regions of the ABoVE domain under SSP126 and SSP585. In each panel, blue and red lines represent the projection under SSP126 and SSP585, separately.

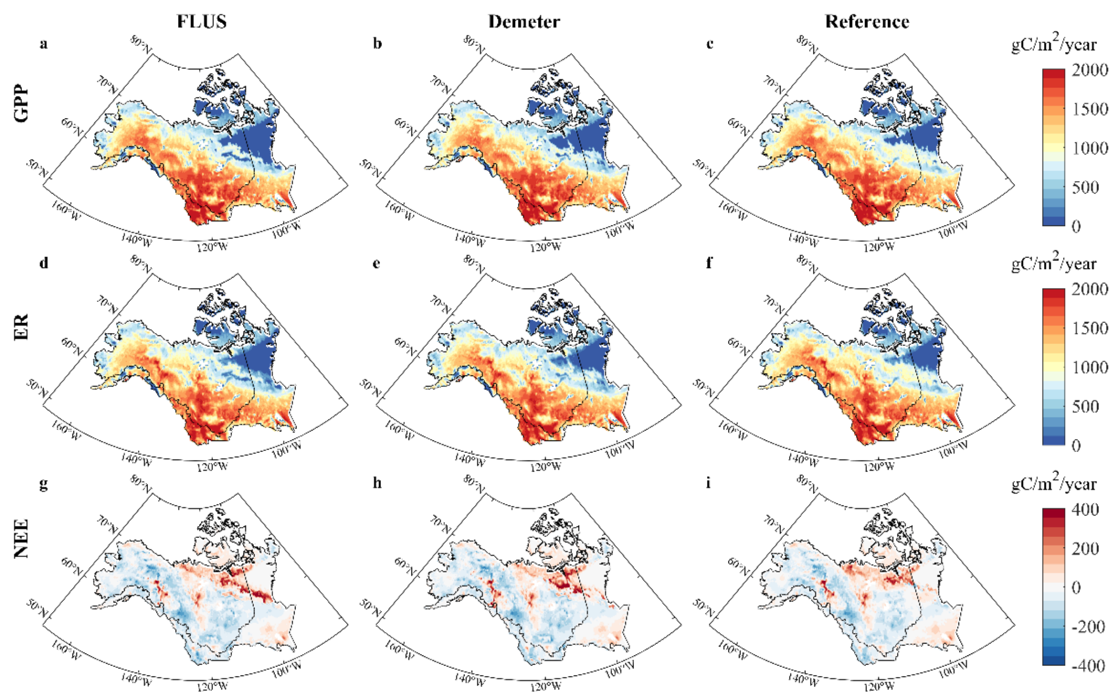

Figure S6. The spatial pattern of (a-c) GPP, (d-f) ER, and (g-i) NEE in 2100 using $LULCC_{FLUS}$, $LULCC_{Demeter}$ and historical LULCC in 2015 under SSP126.

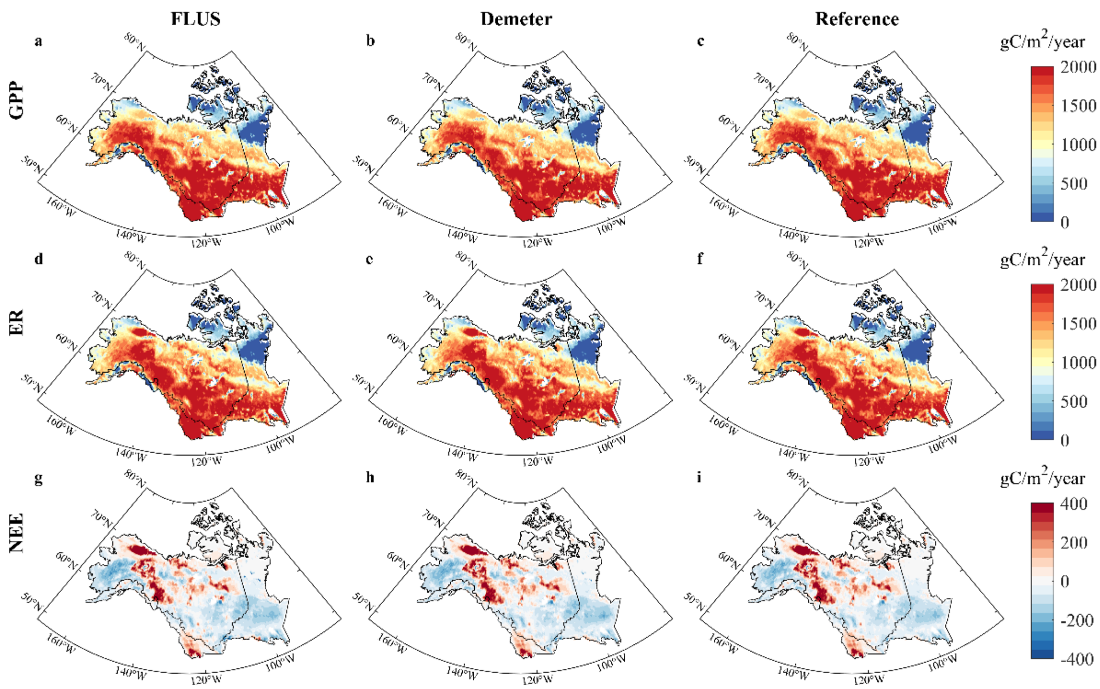

Figure S7. The spatial pattern of (a-c) GPP, (d-f) ER, and (g-i) NEE in 2100 using $LULCC_{FLUS}$, $LULCC_{Demeter}$ and historical LULCC in 2015 under SSP585.

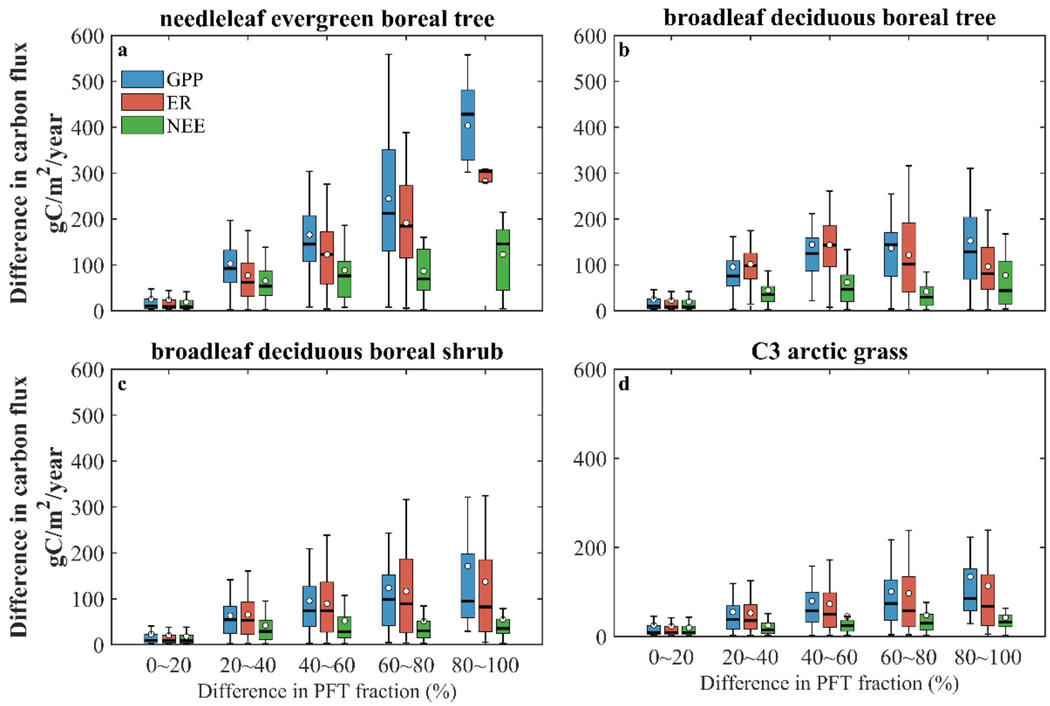

Figure S8. The relationship of the absolute difference in PFT fraction between $LULCC_{FLUS}$ and $LULCC_{Demeter}$ with the absolute difference in GPP (blue), ER (red), and NEE (green) under SSP585 for 4 PFTs: (a) needleleaf evergreen boreal tree, (b) broadleaf deciduous boreal tree, (c) broadleaf deciduous boreal shrub, and (d) C3 arctic grass.

Table S1. *Statistical differences in GPP, ER, and NEE between the simulations using $LULCC_{Demeter}$ and $LULCC_{FLUS}$ separately, in 2100 under SSP126 and SSP585.*

	SSP126 RMSD (gC/m²/year)	Bias (gC/m²/year)	SSP585 RMSD (gC/m²/year)	Bias (gC/m²/year)
GPP	120.9	1.7	53.3	-4.6
NEE	107.4	1.9	44.9	0.6
ER	53.3	0.1	29.7	4.0